REPORT DOCUMENTATION PAGE

Form Approved
OMB No 0704-0188

Public reporting burden for this collection of information is estimated to average 1 hour per response, including the time for reviewing instructions, searching existing data sources, gathering and maintaining the data needed, and completing and reviewing the collection of information. Send comments regarding this burden estimate or any other aspect of this collection of information, including suggestions for reducing this burden, to Washington Headquarters Services, Directorate for Information Operations and Reports, 1215 Jefferson Davis Highway, Suite 1204, Arlington, VA 22202-4302, and to the Office of Management and Budget, Paperwork Reduction Project (0704-0188), Washington, DC 20503.

1. AGENCY USE ONLY (Leave blank)	2. REPORT DATE 31 MAY 95	3. REPORT TYPE AND DATES COVERED FINAL Feb. 1, 1994 – May 31, 1995

4. TITLE AND SUBTITLE Dynamics, Control and Maneuvering of Large Flexible Space Tethered Reflectors, Tele-robots and Experimental Models – Part II	5. FUNDING NUMBERS CF 49620-92J-0165

6. AUTHOR(S) Peter M. Bainum, Feiyue Li, Jianke, Xu, Tan Zhao Zhi, Xing Guang-qian, and Raj Kotaru

AFOSR-TR-95

0530

7. PERFORMING ORGANIZATION NAME(S) AND ADDRESS(ES)

Howard University
Dept. of Mechanical Engineering
Washington, D.C.   20059

9. SPONSORING/MONITORING AGENCY NAME(S) AND ADDRESS(ES)

Air Force Office of Scientific Research   NA
AFSC/NA
Bolling AFB, D.C.   20332-6448

10. SPONSORING/MONITORING AGENCY REPORT NUMBER
F49620-92-J-0165

11. SUPPLEMENTARY NOTES

DTIC SELECTED
AUG 22 1995
B

12a. DISTRIBUTION/AVAILABILITY STATEMENT

Approved for public release; distribution is
unlimited.

12b. DISTRIBUTION CODE

13. ABSTRACT (Maximum 200 words)   The effects of solar radiation heating on a large thin, shallow spherical orbiting shell system are studied. After determining the steady state temperature distribution across the thickness of the shell, the corresponding thermal deformation is estimated as a function of the solar incidence angle and material properties. The closed-loop dynamic response of the shell is simulated by using LQR control design synthesis and assuming that 12 point actuators are placed on the outer surface and edge of the shell. The shell's transverse elastic vibrational frequencies may differ significantly from their nominal values due to the solar-thermal influence.

A practical control strategy for the minimum-time maneuver problem has been developed and successfully applied to the Naval Research Laboratory's Reconfigurable Spacecraft Host for Attitude and Pointing Experiments (RESHAPE) hardware test facility. This is the first time that the bang-bang type and feedback control strategy has been applied to the RESHAPE facility by including a flexible appendage. The tests resulted in an excellent correlation between the numerical simulations and the experimental test results.

14. SUBJECT TERMS solar-thermal disturbances; LQR control; three-axis, near time-optimal maneuver experiments with flexibility; feed forward and feedback control.	15. NUMBER OF PAGES 61
	16. PRICE CODE

17. SECURITY CLASSIFICATION OF REPORT	18. SECURITY CLASSIFICATION OF THIS PAGE	19. SECURITY CLASSIFICATION OF ABSTRACT	20. LIMITATION OF ABSTRACT
unclassified	unclassified	unclassified	UL

NSN 7540-01-280-5500

Standard Form 298 (Rev. 2-89)
Prescribed by ANSI Std. Z39-18
298-102

19950821 042

ACKNOWLEDGEMENT

iii

ABSTRACT

The effects of solar radiation heating on a large, thin, shallow spherical orbiting shell system are studied. The shell is representative of a large antenna /reflector system which could also be gravitationally stabilized by connecting a sub-satellite to a long tether. After determining the steady state temperature distribution across the thickness of the shell, the corresponding thermal deformation is estimated as a function of the solar incidence angle and material properties. The closed-loop dynamic response of the shell is simulated by using LQR control design synthesis and assuming that 12 point actuators are placed on the outer surface and edge of the shell. Calculations also indicate that the shell's transverse elastic vibrational frequencies may differ significantly from their nominal values due to the solar-thermal influence.

A practical control strategy for the minimum-time maneuver problem has been developed and successfully applied to the Naval Research Laboratory's Reconfigurable Spacecraft Host for Attitude and Pointing Experiments (RESHAPE) hardware test facility. This is the first time that the bang-bang type and feedback control strategy has been applied to the RESHAPE facility by including a flexible appendage which is represented with the attachment of a spherical pendulum device to the edge of the RESHAPE platform. The tests resulted in an excellent correlation between the numerical simulations and the experimental test results, and demonstrates the effectiveness of the feed forward and state-error feedback control strategy.

TABLE OF CONTENTS

I. INTRODUCTION

A tethered reflector/antenna system has been suggested for possible use in mobile communications, power transmission and astronomical observations and has been the subject of study in several past AFOSR grant reports. The tether would be attached to a large orbiting antenna/reflector and also to a small subsatellite. For communications and power generation the subsatellite could contain the electronic feed or power generating system. The system could be gravitationally stabilized by deploying a small (200-500 kg.) subsatellite a distance of 1km downward along the local vertical.

The second chapters of this report extends the previous analyses of the effect of environmental disturbances due to solar radiation pressure to now include the heating attributed to the thermal gradients which result in thermally induced deformations. In many cases there will be a noticeable interaction between the solar radiation pressure and the thermally distorted system. In this chapter the dynamics and control of an orbiting shallow spherical shell subject to solar-thermal interaction is studied. Expressions for the thermal deflections and resulting solar radiation pressure induced torques are developed. Control of the orientation and shape of the shell can be accomplished by the use of actuators located at certain points on the shell surface and outer edge.

In last year's grant report the successful testing of three-axes near minimum time maneuvers using the Naval Research Laboratory's Reconfigurable Spacecraft Host for Attitude and Pointing Experiments (RESHAPE) was reported. An excellent correlation between numerically calculated and experimentally obtained results was accomplished. These previous results were based on a rigidized model of the RESHAPE platform representative of three-axis

maneuvers of a rigid spacecraft system. Recently these results have been extended by utilizing a pendulum attached vertically by a string to the edge of the RESHAPE's circular platform which could represent a flexible appendage. The first degree of freedom of the pendulum can be described by a swing motion with respect to a vertical line through the attachment point in the tangential plane, and represents the first flexible appendage mode. A second degree of freedom is represented by the out-of-the tangential plane angular motion. In Chapter Three of this report the recent numerical and experimental results of near-minimum time maneuvers of the NRL RESHAPE test facility with the flexible pendulum appendage are described. The control strategy is based on the feedforward (open-loop solution) plus the state-error feedback control; this strategy has been successfully used in the previous experimental study based on the rigid-model of the RESHAPE. This is the first time that a bang-bang type and feedback control strategy has been applied to the RESHAPE testing facility with a flexible appendage included.

Finally Chapter Four summarizes the over-all conclusions and suggestions for further work.

II. SOLAR - THERMAL EFFECTS ON A SHALLOW SPHERICAL SHELL IN ORBIT

Abstract

The effects of solar radiation heating on a large, shallow, spherical shell in orbit are considered. After determining the steady state temperature distribution across the shell thickness, the thermal deformation experienced is estimated as a function of the material properties and the solar incidence angle. There is a harmonic variation of the physical dimensions of the shell as a function of orbital position. The dynamic response of the shell is simulated by utilizing a configuration of twelve control actuators placed on its outer surface and on its edge, and utilizing the LQR design methodology. More significantly, calculations show that the frequencies of transverse vibrations of the shell elastic modes experience considerable deviation from their nominal values due to solar-thermal effects. This shift in the frequencies must be taken into consideration, for large shells which are inherently flexible.

2.1 Introduction

The effect of environmental disturbing influences on large space structures in orbit has received a great deal of attention in recent years. The major environmental disturbances on such structures will be due to solar radiation pressure and solar heating. The use of thin, shallow, spherical, shell type structures as principal components of large space structures is also quite widespread. In particular, shallow spherical shell type structures may be used as reflectors or antennas to perform various tasks in such disciplines as telecommunications, astronautics, space exploration, etc. The effect of solar radiation pressure acting as a load on a class of flexible shallow, spherical shell type structures has been considered previously[1]. It was determined that the solar radiation pressure interacts with the elastic modes of the shell to produce significantly higher rigid modal oscillations as compared to the oscillations produced if the shell were treated as completely rigid. Another important environmental effect is the heat due to solar radiation that results in thermal gradients in a structure. For specific materials, the thermal, mechanical, and surface properties are such that the deformations that are caused by thermal gradients can sometimes result in dynamic instability of the orbiting structure[2]. In most cases, there is also a significant interaction between the solar radiation pressure and the thermally deformed structure. The dynamics of orbiting beams and plates in the presence of such a solar-thermal interaction has also been investigated[3]. In this paper, the dynamics of an orbiting shallow spherical shell subjected to such an interaction will be studied. Expressions for the thermal deflection of a spherical shell will be developed. The solar radiation pressure torque acting on such a thermally deformed shell will be estimated and an attempt will be made to control the attitude of the shell by means of actuators strategically placed on its outer surface and on the edge. Finally, the extent of any thermoelastic interaction will be investigated by considering the shift in the natural frequencies of the shell flexible modes as a result of the solar-thermal interaction.

2.2 Assumptions

The general problem of solar-thermal interaction and the associated thermoelastic problem is very complicated for structures that span more than one dimension. The problem becomes even more complicated if thermal transients, the shadowing of the structure and the non-linear boundary conditions associated with radiation heat-transfer from the exposed surfaces are all taken into account. In the present analysis, the following simplifying assumptions are made in order to reduce the problem to manageable proportions.

1. The thin, shallow, spherical shell is assumed to move in a 100% sunlit, circular orbit at a geosynchronous altitude. Furthermore, solar radiation is restricted to the plane of the orbit.
2. The effects of the Earth reflected solar radiation and the thermal radiation emanating from the Earth are neglected.
3. The inherent time lags in the heat transfer process are very small compared with the orbital period ($\approx$ 24 hours for a geosynchronous orbit) and are ignored.
4. Owing to the small thickness of the shell, the radiation from its edge can be neglected.
5. The local shadowing of a part of the shell due to the remaining part can be neglected because of the extreme shallowness of the shell.
6. The steady state temperature distribution is strictly a function of the radial coordinate. Thus, the temperature varies only along the shell thickness. This necessarily implies that at steady state, the isothermal surfaces are concentric spheres. Another implication of this assumption is that no shear stresses are introduced as a result of the thermal gradient. As a consequence, the thermal deflection will have a lone radial component.
7. For the simulation times (2-3 orbit periods) considered in the analysis, it will be assumed that the position of the Sun remains fixed with respect to an Earth-fixed inertial frame of reference.

2.3 The Thermal Problem

The equation that governs the conduction of heat in a spherical domain is given by:

$$\frac{\partial T}{\partial t} = \kappa \nabla^2 T = \kappa \left(\frac{\partial T^2}{\partial r^2} + \frac{2}{r} \frac{\partial T}{\partial r} \right) \tag{1}$$

where, κ is the thermal diffusivity, r is the radial coordinate (along the shell thickness), t denotes time and $T = T(r,t)$ is the temperature. The steady state temperature distribution, is given by:

$$r \frac{d^2 T}{dr^2} + 2 \frac{dT}{dr} = 0 \tag{2}$$

The solution to (2) can be achieved[4], by changing the dependent variable to rT. If r_o, r_i, and T_o, T_i

respectively denote the radii of curvature and the steady temperatures at the outer and inner surfaces of the shell, then it can be easily shown that:

$$T(r) = \frac{T_i r_i (r_o - r) + T_o r_o (r - r_i)}{r(r_o - r_i)}$$

(3)

Fig. 1. shows the cross-sectional geometry of the shallow spherical shell along with it dimensions. Fig. 2. shows the cross-section of the shell in the orbit plane in a state of thermal equilibrium. Here, **t**, denotes the unit vector in the direction of the incoming solar flux, making an instantaneous angle of θ_i with the outward normal to the shell. The solar incidence angle θ_i, is assumed to be a constant for a small interval of time. During this interval, the surface facing the sun, S_o, attains a steady state temperature T_o, while the surface away from the sun, S_i, attains a steady state temperature T_i. The total heat leaving the shell from the two surfaces should equal the heat received by the shell from the solar flux. At equilibrium, the heat flowing through the shell along the radial direction must also equal the heat radiated from the unexposed surface of the shell. The above two statements represent heat energy balance equations, the mathematical equivalents of which will be used to solve for the steady state temperatures attained by the outer and the inner surfaces of the shell.

If e_o and e_i respectively denote the emissivities of the outer and the inner surface of the shell, σ, the Stefan-Boltzmann constant ($=56.7 \times 10^{-12}$ KW/m^2-K^4), k, the coefficient of thermal conductivity of the shell material, h, the nominal value for the thickness of the shell, α_s, the absorptivity coefficient of the exposed shell surface, and G, the intensity of solar radiation (≈ 0.8 KW/m^2) for Earth-orbiting structures, then the above mentioned statements of thermal equilibrium result in:

$$e_o \sigma T_o^4 + e_i \sigma T_i^4 = \alpha_s G \cos\theta_i(t)$$
$$e_i \sigma T_i^4 = \frac{k(T_o - T_i)}{h}$$

(4)

when the outer surface of the shell is exposed to solar radiation and,

$$e_i \sigma T_i^4 + e_o \sigma T_o^4 = \alpha_s G \cos\theta_i(t)$$
$$e_o \sigma T_o^4 = \frac{k(T_i - T_o)}{h}$$

(5)

When the inner surface of the shell is exposed to solar radiation. In the present analysis, depending on the instantaneous (angular) location of the shell in its orbit, the set of equations represented by either (4) or (5) will be used to numerically solve for the steady state temperatures attained by the inner and outer surfaces. The Newton-Raphson algorithm will be used for this purpose. It is clear from (4) and (5) that the amount of thermal radiation received by the shell from the sun is greatest when the outward normal vector to the exposed shell surface and the unit

2.3

vector in the direction of the incoming solar flux are parallel to each other. This occurs (when θ_i =0), twice per orbit. It is reasonable to expect that the thermal gradient, $| T_o - T_i |$ will be greatest at these two locations. The results can be seen in Fig. 3, which shows the steady state surface temperatures as a function of time, for a shell made up of polyamide ($k = 0.245 \times 10^{-3}$ KW/m-^{0}K) and when $e_o = e_i = 0.05$ and $\alpha_s = 0.2$. It can be seen that for each orbit, the only period of time when the inner surface attains a steady state temperature greater then the steady state temperature of the outer surface is when the inner surface is exposed to the sun.

2.4 Thermal Deformation

With the assumption that the temperature varies only along the radial direction, it can be demonstrated[5] that the thermal deflection is also a function of the radial coordinate r. Figure 4, shows an infinitesimal element of the shallow spherical shell in a state of spherically symmetric stress. It can be demonstrated[5], that under these conditions all shear stress components vanish and $\sigma_\theta = \sigma_T = \sigma_\phi$ which will be referred to as the tangential stress component. Utilizing the stress equilibrium equations, the stress-strain constitutive relations and the strain-displacement field equations in the spherical domain, it can be shown that[5]:

$$\sigma_r(r) = -\frac{2E}{1-\nu}\frac{1}{r^3}\int_{\rho=r_i}^{\rho=r}\rho^2\alpha T(\rho)\,d\rho + \frac{E}{1-2\nu}A - \frac{2E}{1+\nu}\frac{B}{r^3}$$

(6)

$$\sigma_T(r) = \frac{E}{1-\nu}\frac{1}{r^3}\int_{\rho=r_i}^{\rho=r}\rho^2\alpha T(\rho)\,d\rho + \frac{E}{1-2\nu}A + \frac{E}{1+\nu}\frac{B}{r^3} - \frac{\alpha TE}{1-\nu}$$

(7)

$$u(r) = \frac{1+\nu}{1-\nu}\frac{1}{r^2}\int_{\rho=r_i}^{\rho=r}\rho^2\alpha T(\rho)\,d\rho + Ar + \frac{B}{r^2}$$

(8)

where, E, ν, and α are respectively the Young's modulus, the Poisson's ratio and the coefficient of linear expansion of the material of the shell. A and B are constants to be determined from the boundary conditions. Using (3) in (8), and making the assumption that α does not vary across the shell thickness, it can be shown that:

2.4

$$u(r) = \frac{1+\nu}{1-\nu} \frac{\alpha}{r^2} \left[\frac{1}{2} \left\{ T_o r_o - \frac{(T_i r_i - T_o r_o) r_o}{r_i - r_o} \right\} (r^2 - r_i^2) \right.$$
$$\left. + \frac{1}{3} \frac{(T_i r_i - T_o r_o)}{r_i - r_o} (r^3 - r_i^3) \right] + Ar + \frac{B}{r^2}$$

(9)

In order to determine A and B one can impose the condition that the normal radial stress components vanish at the inner and outer surfaces.

$$\sigma_r(r_i) = \sigma_r(r_o) = 0$$

(10)

Using (3) in (6) results in,

$$\sigma_r(r) = -\frac{2E}{1-\nu} \frac{\alpha}{r^3} \left[\frac{1}{2} \left\{ T_o r_o - \frac{(T_i r_i - T_o r_o) r_o}{r_i - r_o} \right\} (r^2 - r_i^2) \right.$$
$$\left. + \frac{1}{3} \frac{(T_i r_i - T_o r_o)}{r_i - r_o} (r^3 - r_i^3) \right] + \frac{E}{1-2\nu} A - \frac{2E}{1+\nu} \frac{B}{r^3}$$

(11)

Using (11) in (10), one can solve for A and B as:

$$A = \frac{1-2\nu}{1-\nu} \frac{2\alpha}{r_o^3 - r_i^3} \left[\frac{1}{2} \left\{ T_o r_o - \frac{(T_i r_i - T_o r_o) r_o}{r_i - r_o} \right\} \right.$$
$$\left. (r_o^2 - r_i^2) + \frac{1}{3} \frac{(T_i r_i - T_o r_o)}{r_i - r_o} (r_o^3 - r_i^3) \right]$$

(12)

$$B = \frac{1+\nu}{1-\nu} \frac{\alpha r_i^3}{r_o^3 - r_i^3} \left[\frac{1}{2} \left\{ T_o r_o - \frac{(T_i r_i - T_o r_o) r_o}{r_i - r_o} \right\} \right.$$
$$\left. (r_o^2 - r_i^2) + \frac{1}{3} \frac{(T_i r_i - T_o r_o)}{r_i - r_o} (r_Q^3 - r_i^3) \right]$$

(13)

Finally, using (12) and (13) in (9) results in:

$$u(r) = \frac{1+\nu}{1-\nu} \frac{\alpha}{r^2} \left[\frac{1}{2} \left\{ T_o r_o - \frac{(T_i r_i - T_o r_o) r_o}{r_i - r_o} \right\} (r^2 - r_i^2) + \right.$$
$$\frac{1}{3} \frac{(T_i r_i - T_o r_o)}{r_i - r_o} (r^3 - r_i^3) \left] + \frac{\alpha}{(1-\nu)(r_o^3 - r_i^3)} \right.$$
$$\left[\frac{1}{2} \left\{ T_o r_o - \frac{(T_i r_i - T_o r_o) r_o}{r_i - r_o} \right\} (r_o^2 - r_i^2) + \right.$$
$$\frac{1}{3} \frac{(T_i r_i - T_o r_o)}{r_i - r_o} (r_o^3 - r_i^3) \left] \left[2(1-2\nu) r + \frac{(1+\nu) r_i^3}{r^2} \right] \right.$$

(14)

Since the isothermal surfaces inside the shell are concentric spheres, (14), gives the radial displacement of the generic isothermal at radius $r \in [r_i, r_o]$. For the problem at hand, the solar radiation pressure torques acting on the thermally deformed shell depend primarily on the radius of curvature of the inner and outer surfaces. Thus, the radial displacements on these surfaces are of special interest. It is easily verified that:

$$u(r_i) = \frac{3\alpha r_i}{r_o^3 - r_i^3} \left[\frac{1}{2} \left\{ T_o r_o - \frac{(T_i r_i - T_o r_o) r_o}{r_i - r_o} \right\} \right.$$
$$\left. (r_o^2 - r_i^2) + \frac{1}{3} \frac{(T_i r_i - T_o r_o)}{r_i - r_o} (r_o^3 - r_i^3) \right]$$

(15)

$$u(r_o) = \frac{3\alpha r_o}{r_o^3 - r_i^3} \left[\frac{1}{2} \left\{ T_o r_o - \frac{(T_i r_i - T_o r_o) r_o}{r_i - r_o} \right\} \right.$$
$$\left. (r_o^2 - r_i^2) + \frac{1}{3} \frac{(T_i r_i - T_o r_o)}{r_i - r_o} (r_o^3 - r_i^3) \right]$$

(16)

The deformation given by (14) will be along the direction of the surface that attains the greater steady state temperature. Because of the symmetric nature of this deformation, the overall effect is to cause an expansion of the interior of the shell without altering its shape. As the shell moves in its orbit, the change in the intensity of solar radiation to which it is exposed causes it to experience periodic heating and cooling phases which alternate once for each orbit (Fig.3). As a consequence of these alternate heating and cooling phases, the shell undergoes periodic expansions and contractions that cause the principal dimensions of the shell (a, r_i, r_o, and, H) to vary, but it retains its spherical shape.

Fig. 5 shows the deformation undergone by the generic isothermal surface at r to a position at r', as dictated by (14). If a', H', and ψ' respectively denote the altered values of the base radius, the height, and the negative of the distance of the center of the center mass from its center of curvature, then from the geometry of Fig. 5, it is obvious that:

$$a' = a\frac{r'}{r} \qquad H' = r' - \sqrt{r'^2 - a'^2} \qquad \psi' = -r' + \frac{H'}{2} \qquad (17)$$

Figures 6,7,8,9 and 10 respectively show the variation of the shell inner radius of curvature, the shell outer radius of curvature, the shell thickness, the shell base radius and the shell height as a function of orbital time. The shell inner and outer radii experience significant variations with time due to solar-thermal effects. A peak deviation of nearly 17 m from the nominal value of 5000 m is observed. Figures 8-10 show that the remaining dimensions of the shell only undergo small changes in magnitude.

2.5 The Solar Radiation Model

The solar radiation pressure torques induced about the center of mass of the deformed shell will form the focus of attention of this section. Expressions for the solar radiation forces and torques acting on space structures of arbitrary shape were derived by Karymov[6]. In the Karymov formulation, solar radiation force and torque expressions are first obtained for the separate cases of totally absorbing and totally reflecting surfaces. If N_a and N_r denote the solar radiation torques on a completely absorbing and a completely reflecting surface, respectively, then,

$$\vec{N}_a = h_o \ \vec{t} \ X \int_S \vec{\rho} \ (\vec{t} . \vec{n}) \ dS$$

$$\vec{N}_r = 2h_o \int_S \vec{n} \ X \ \vec{\rho} \ (\vec{t} . \vec{n})^2 dS \qquad (18)$$

Where, h_o is the solar radiation constant $= 4.64 \times 10^{-6}$ N/m^2, t is the unit vector in the direction of the incoming solar flux, ρ is the position vector of the generic point on the shell surface from its center of mass, n is the outward unit normal vector at the generic point, and dS is the area of the infinitesimal element on the deformed shell surface. The integration in (18) is over the surface of the structure that is actually exposed to solar radiation and is bounded by the condition $t.n \leq 0$. Fig. 11 shows a shell with outer radius of curvature R and the coordinate frame used to model solar radiation effects. The origin of the coordinate frame is at the instantaneous center of curvature of the shell and the z-axis is aligned with its symmetry axis. From Fig. 11, the following expressions can be obtained:

$$\vec{\rho} = R\sin\phi\cos\theta \ \vec{i} + R\sin\phi\sin\theta \ \vec{j} + (R\cos\phi + \psi) \ \vec{k}$$
$$\vec{t} = -\sin\alpha\cos\beta \ \vec{i} - \sin\alpha\sin\beta \ \vec{j} - \cos\alpha \ \vec{k}$$
$$\vec{n} = \cos\theta\sin\phi \ \vec{i} + \sin\theta\sin\phi \ \vec{j} + \cos\phi \ \vec{k} \qquad (19)$$
$$dS = R^2\sin\phi \ d\theta d\phi$$

Where α and β are the two solar incidence angles that uniquely fix the orientation of t, and (R,θ,ϕ) are the spherical coordinates associated with a generic point on the shell surface. Using (10) in (18), one can derive the following expressions for the solar radiation torques:

$$N_{ax} = \Pi h_o R^2 s\alpha c\alpha s\beta [R(c\phi_o - c^3\phi_o) + \psi s^2\phi_o]$$
$$N_{ay} = \Pi h_o R^2 s\alpha c\alpha c\beta [R(c^3\phi_o - c\phi_o) - \psi s^2\phi_o] \tag{20}$$
$$N_{az} = 0$$

$$N_{rx} = \Pi h_o R^2 \psi s\alpha c\alpha s\beta s^4\phi_o$$
$$N_{ry} = -\Pi h_o R^2 \psi s\alpha c\alpha c\beta s^4\phi_o \tag{21}$$
$$N_{az} = 0$$

Here, ϕ_o denotes the constant apex angle of the shell. Furthermore, since the unit vector in the direction of the incoming solar flux is assumed to lie entirely within the orbit plane, $\beta = \pi/2$ will have to be used in (20) and (21). With this assumption, the solar radiation pressure induces a torque only about the pitch axis of the shell. In the Karymov formulation, the overall solar radiation torque acting on a shell whose surface has an arbitrary coefficient of reflectivity, e, is given by:

$$\vec{N} = (1-e)\vec{N}_a + e\vec{N}_r \tag{22}$$

As the shell moves about in its orbit, the solar radiation torques induced (equations (20)-(21)) vary not only because of a variation in the solar incidence angles α and β, but also because of a variation in the dimensions of the shell due to thermal effects (Figures 6-10). Figures 12 and 13 show the variation of the solar radiation torque acting about the pitch axis for the cases of a shell with a completely absorbing and a completely reflecting surface, respectively. Also shown in these figures is the variation of the torques when the thermal deformation of the shell is not considered. The figures demonstrate that the inclusion of thermal deformation effects, results only in a negligible increase in the solar radiation torque induced.

2.6 Equations of Motion

The equations of motion of an orbiting shallow spherical shell were derived by Bainum and Kumar[7]. The linearized equations of a completely rigid shell can be shown to be:

$$q_x'' - 3\Omega_x q_x = \frac{C_x}{J_x \omega_c^2}$$

$$q_y'' + 4\Omega_y q_y + (1 - \Omega_y) q_y' = \frac{C_y}{J_y \omega_c^2} \tag{23}$$

$$q_z'' - \Omega_z q_z - (1 + \Omega_z) q_z' = \frac{C_z}{J_z \omega_c^2}$$

Here q_x, q_y, and q_z respectively denote the shell pitch, roll, and yaw. J_x, J_y, and J_z denote the mass

moments of inertia of the shell about the axes of the reference frame of Fig. 11. C_x, C_y, and C_z denote the external torques acting about the axis denoted by the subscript. The attitude of the shell is assumed to be controlled by means of 12 actuators placed on the surface and on the edge of the shell in the configuration of Fig. 14. In Fig. 14, all actuators not on the edge of the shell produce forces directed along the normal to the surface at the point, whereas all actuators on the edge produce forces that have equal components along the normal to the surface, and along the tangent to the edge. Thus, the contribution to the external torques C_x, C_y, C_z in (23) is due to the solar-thermal effects as well as the restoring torques produced by the actuators. The equations of motion given by (23) are rewritten in state-space form as $x' = A_1 x + B_1 u$, and a full state feedback control law of the form $u = -Kx$, that minimizes the performance index:

$$J = \int_0^\infty x^T Q x + u^T R u \; dt \tag{24}$$

is sought. Here, A_1 and B_1 are the state and the control influence matrices, respectively, while Q and R are their corresponding weighting matrices. Using $Q = 100\, I_{6X6}$, and $R = I_{12X12}$, the controlled response of the orbiting shell is simulated and the response of the pitch, the roll, and the yaw obtained is shown in Figures (15), (16), and (17) respectively.

2.7 Effect on Flexibility

The flexibility of the shell is modelled by assuming that the orbiting shell vibrates primarily along the transverse direction. The transverse elastic vibrations of a thin, shallow, spherical shell with a completely free edge were first derived by Reissner and Johnson[8]. They derive expressions for the natural frequencies and mode shapes of the shell and show that each mode shape is uniquely associated with a pair of integers (n,k), where n and k refer to the number of nodal meridians and circles, respectively. Furthermore, the frequency of vibration, $\omega_{n,k}$, of the (n,k)th mode is related to a frequency parameter $\mu_{n,k}$ according to the relation:

$$\omega_{n,k}^2 = \frac{D}{h\rho a^4}\left[\mu_{n,k}^4 + \frac{Ca^4}{DR^2}\right] \tag{25}$$

where h is the shell thickness, ρ is the mass density, and E is the Young's modulus of the shell material. $C = Eh$ is the longitudinal stiffness factor, and $D = Eh^3/12(1 - v^2)$, the bending stiffness factor, with v denoting the Poisson's ratio of the shell material. It can also be demonstrated[8], that for the first few modes (for which the shell vibrates with zero or one nodal meridian) the frequency parameter, $\mu_{n,k}$ satisfies:

$$\frac{\mu_{n,k}}{2}\left[\frac{J_n(\mu_{n,k})}{J_{n+1}(\mu_{n,k})} + \frac{I_n(\mu_{n,k})}{I_{n+1}(\mu_{n,k})}\right] = 1 - v \tag{26}$$

2.9

which must be numerically solved for $\mu_{n,k}$. Here, $J_n(.)$ and $I_n(.)$, respectively denote the Bessel function and the modified Bessel function of the first kind of order n. Equation (25) can then be used to solve for the frequency of vibration $\omega_{n,k}$. In the context of the present problem, the variation of the physical dimensions of the shell from solar-thermal effects causes a shift in the natural frequencies of its elastic modes. Figures (18)-(23) show the variation of $\omega_{n,k}$ with time for the first few modes. Also shown in the figures is the nominal value of $\omega_{n,k}$ for the specific mode. For the dimensions of the shell considered, these nominal values of the frequencies are quite closely packed. Consequently, there is a significant shift in the frequencies from the deformation caused by solar-thermal effects. In fact, for most of the first few modes, it is observed that the peak value of the frequency attained is actually larger than the nominal frequency of the next mode.

2.8 Conclusions

In this paper, a simple mathematical model that incorporates the solar-thermal effects on an orbiting shell has been presented. It has been demonstrated that for a shell made up of polyamide, a peak thermal gradient of nearly 3.6 °C is observed across the 1 cm shell thickness. The shell is alternately heated and cooled in its orbit in a periodic fashion due to a periodic change in the amount of solar radiation to which it is exposed. The shell experiences a peak increase in its radius of curvature of nearly 17 m along with smaller increases in its other dimensions. Although these changes in the dimensions do not significantly increase the solar radiation torque acting on the shell, they cause a significant variation in the frequencies of vibration of the shell flexible modes. This suggests that in the process of the design of control laws of large flexible shells, particular emphasis must be placed in controlling the transverse vibrations. This is particularly true when mission requirements dictate that stringent pointing accuracies be satisfied.

References

1. Kotaru, R. and Bainum, P.M., **"On the Dynamics and Control of an Orbiting Flexible Shallow Spherical Shell in the Presence of Solar Radiation,"** Proceedings of the IX Virginia Polytechnic and State University Symposium on the Dynamics and Control of Large Structures, Blacksburg, VA, May 10-12, 1993, pp. 421-432. Also, The Journal of the Astronautical Sciences, Vol. 42, No. 4, October-December 1994, pp. 395-419.

2. Frisch, H.P., **"Thermally Induced Response of Flexible Structures: A method of Analysis,"** Journal of Guidance and Control, Vol. 3, Jan.-Feb. 1980, pp. 92-94.

3. Krishna, R., and Bainum P.M., **"Dynamics and Control of Orbiting Flexible Structures Exposed to Solar Radiation,"** Journal of Guidance, Control and Dynamics, Vol. 8, No. 5, Sept.-Oct. 1985, pp. 591-596.

4. Carslaw, H.S., "**Introduction to the Mathematical Theory of the Conduction of Heat in Solids**," Dover Publications, New York, 1945, pp. 135-136.

5. Boresi, A.P., "**Elasticity in Engineering Mechanics**," Prentice-Hall, Inc., Englewood Cliffs, New Jersey, 1965, pp. 227-229.

6. Karymov, A.A., "**Determination of Forces and Moments Due to Light Pressure Acting on a Body in Motion in Cosmic Space**," Prikladnaia Matematica I Mechanika (English Translation of the Original Russian Article), Vol. 26, No. 5, 1962, pp. 867-876.

7. Kumar V.K., and Bainum P.M., "**Motion of a Flexible Shallow Spherical Shell in Orbit**," AIAA Journal, Vol. 20, No. 8, Aug. 1982, pp. 1113-1119.

8. Reissner, E., and Johnson M.W., "**On Transverse Vibrations of Shallow Spherical Shells**," Quarterly of Applied Mathematics, Vol. 15, No. 4, 1958, pp. 367-380.
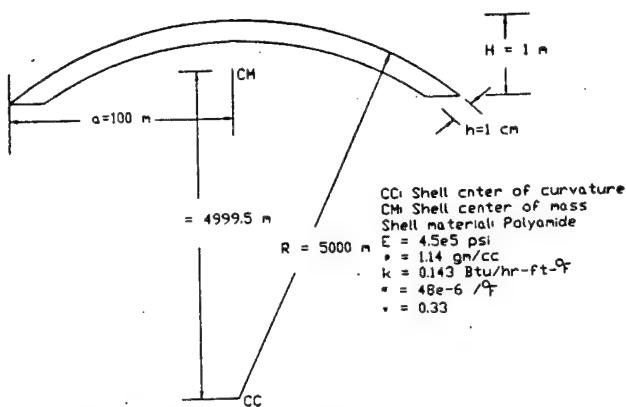
Fig. 1. Shell Cross-Sectional Geometry
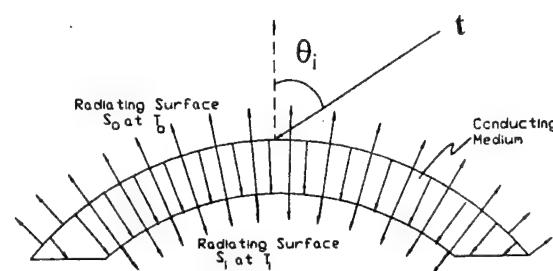
Fig. 2. Thermal Gradient Across Shell Thickness Due to Solar Radiation Heating
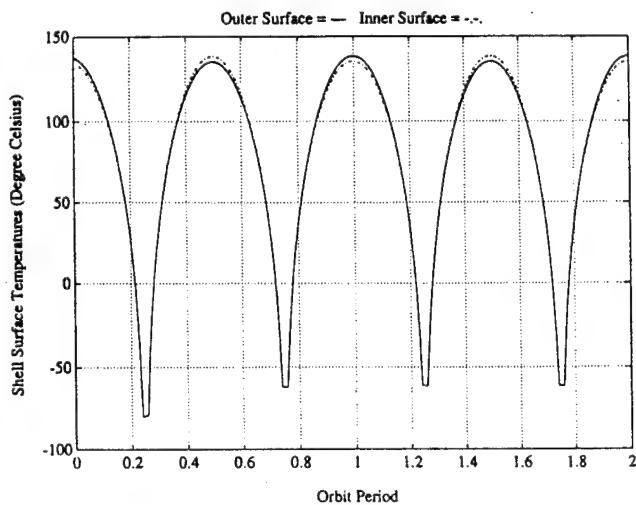
Fig. 3. Variation of Steady State Surface Temperatures
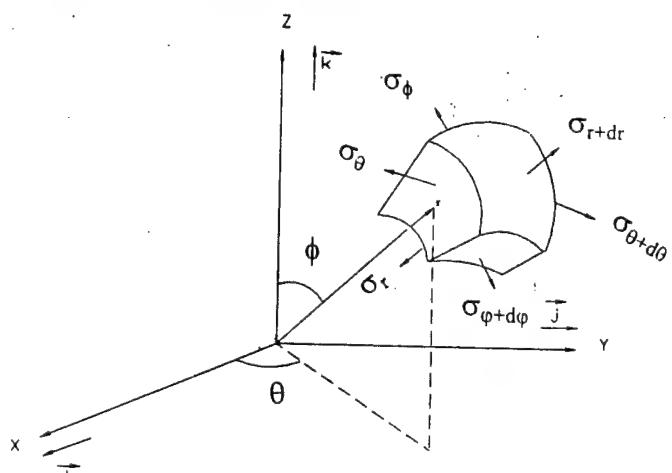
Fig. 4. Stress Distribution on an Infinitesimal Element in the Shell Interior
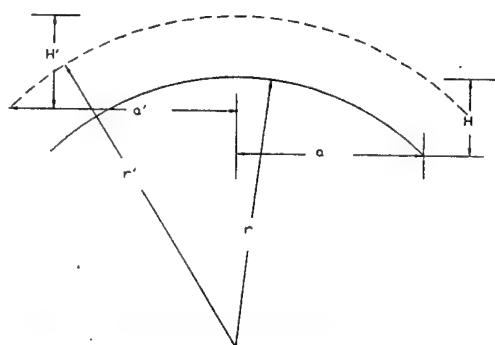
Fig. 5. Thermal Deformation of the generic Isothermal
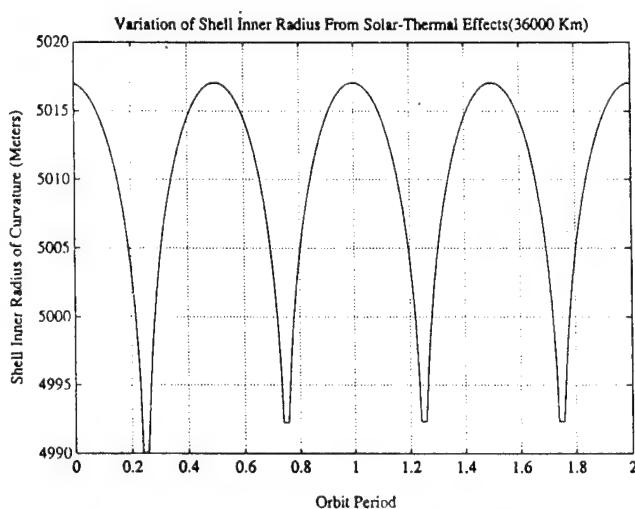
Fig. 6. Shell Inner Radius Vs. Orbital Time

2.12
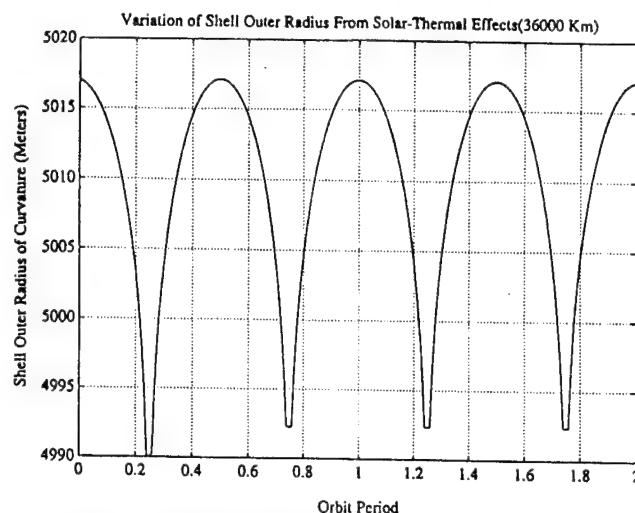
Fig. 7. Shell Outer Radius Vs. Orbital Time
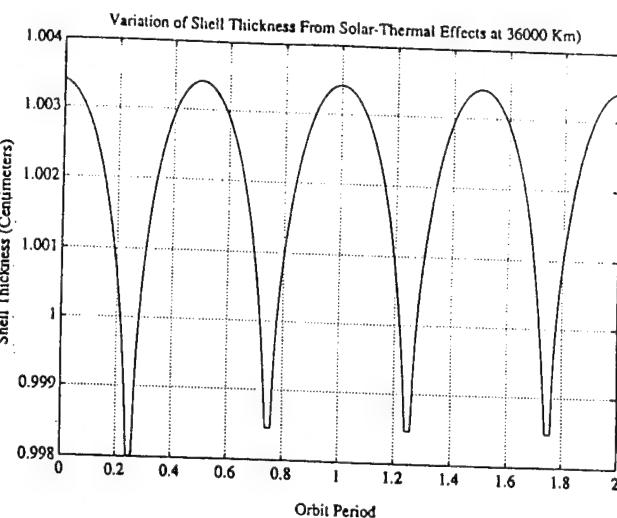
Fig. 8. Shell Thickness Vs. Orbital Time
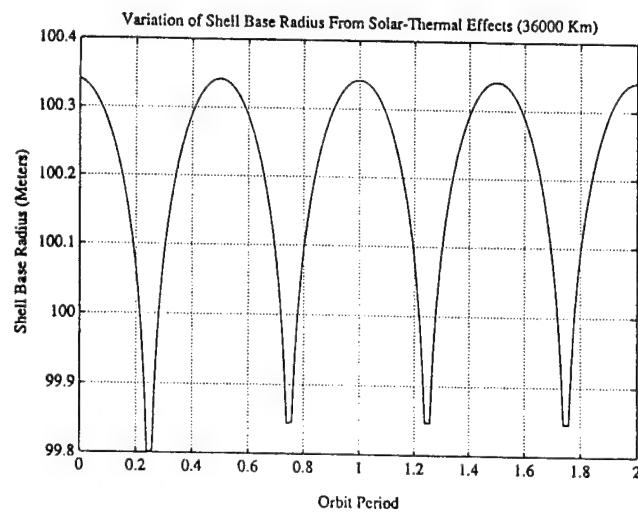
Fig. 9. Shell Base Radius Vs. Orbital Time
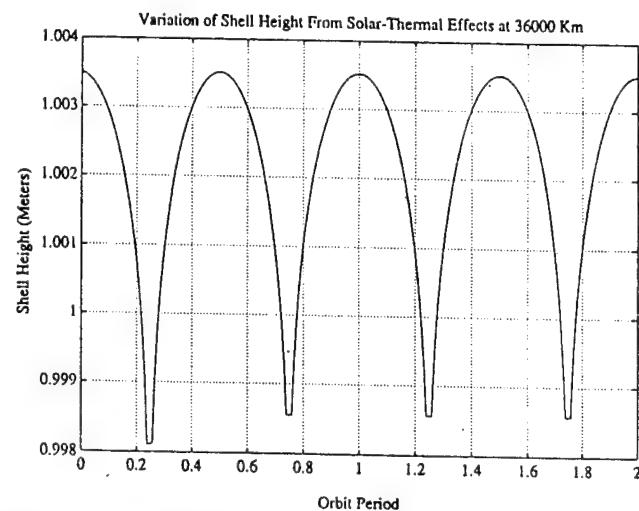
Fig. 10. Shell Height Vs. Orbital Time
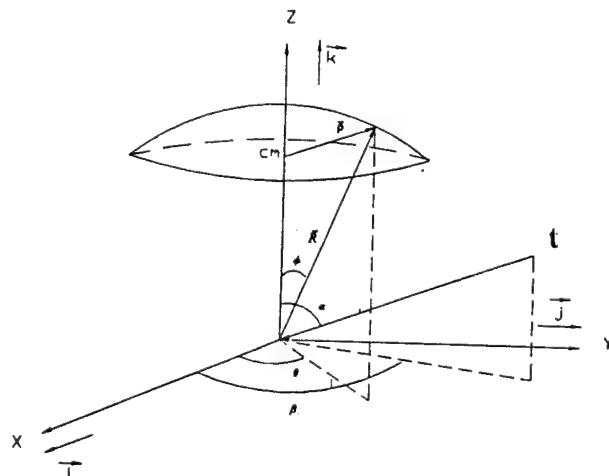
Fig. 11. Reference Frame Used to Model
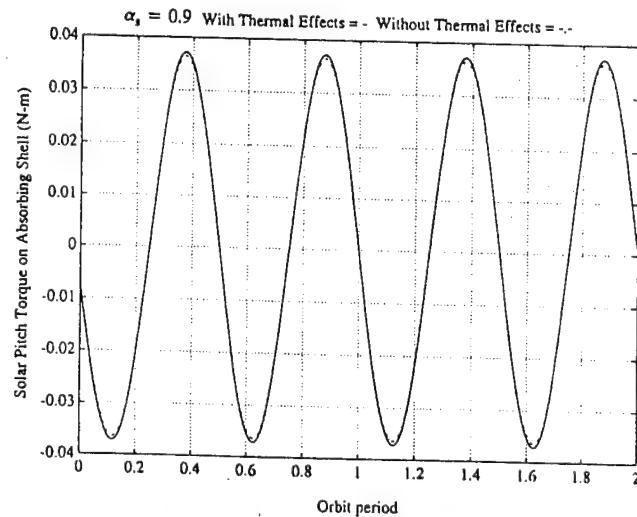
Fig. 12. Solar Heating Effects on Pitch Torque

2.13
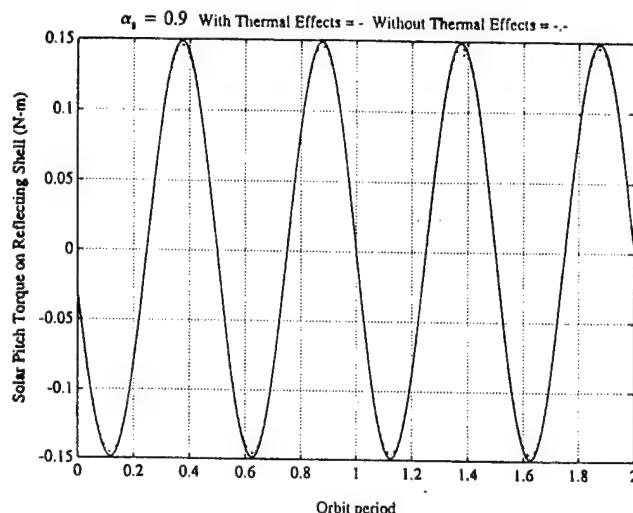
Fig. 13. Solar Heating Effects on
Pitch Torque
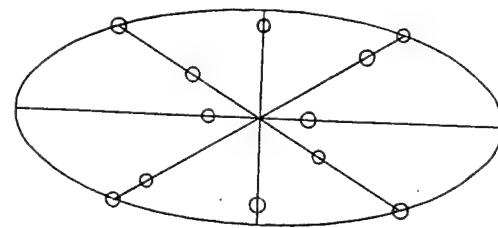
Fig. 14. The Twelve Actuator Configuration
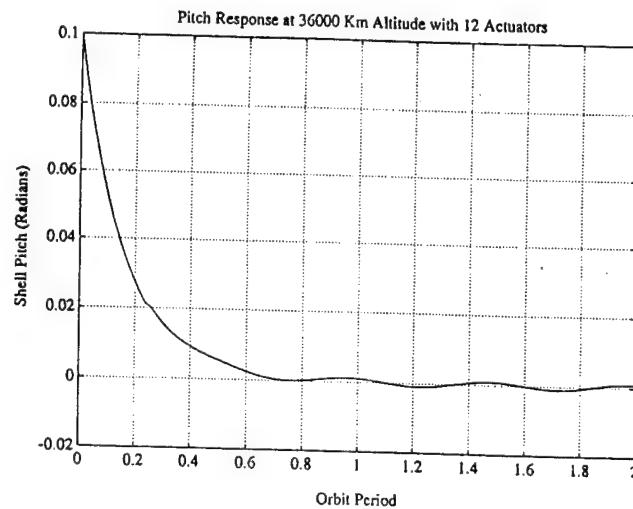
Fig. 15. Shell Pitch Response
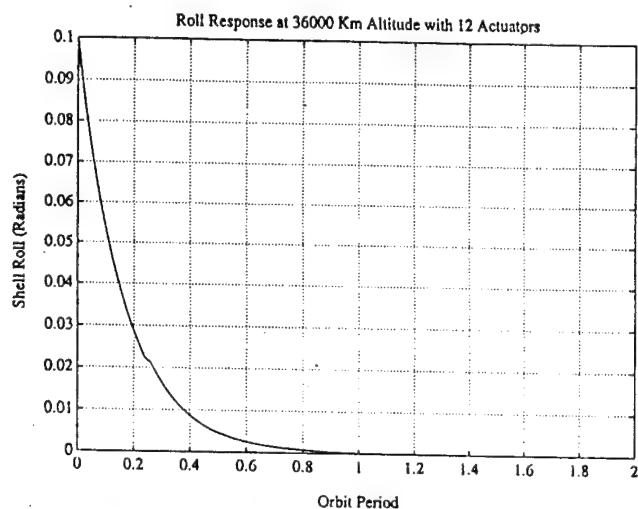
Fig. 16. Shell Roll Response
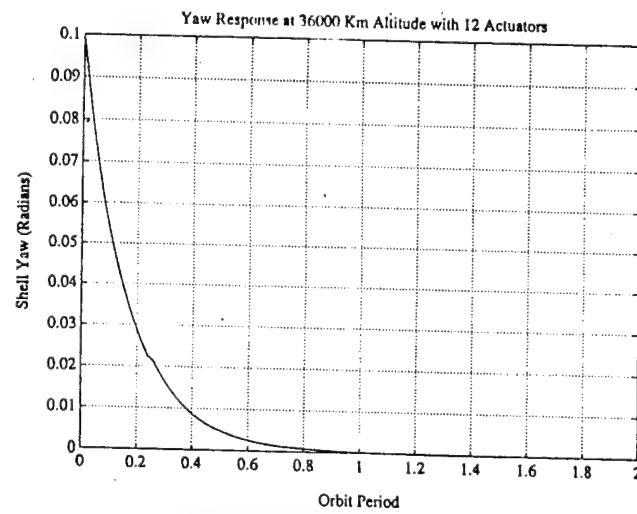
Fig. 17. Shell Yaw Response
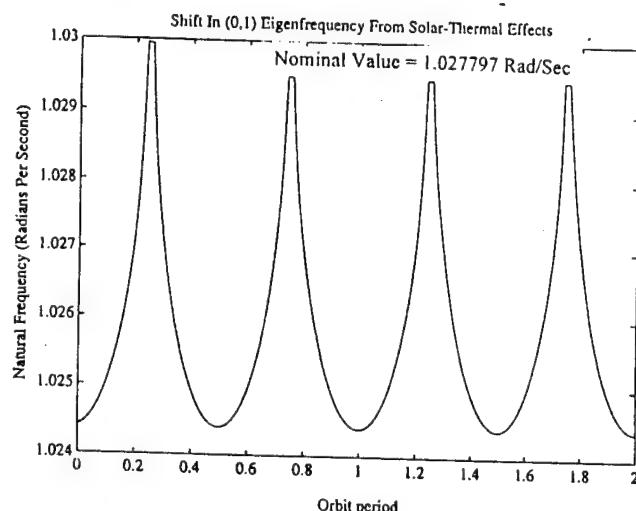
Fig. 18. Shell (0,1) Modal Frequency
Vs. Orbital Time

2.14
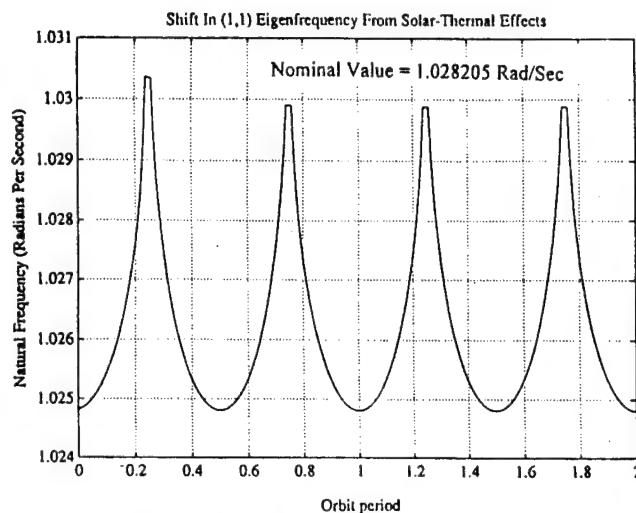
Fig. 19. Shell (1,1) Modal Frequency
Vs. Orbital Time
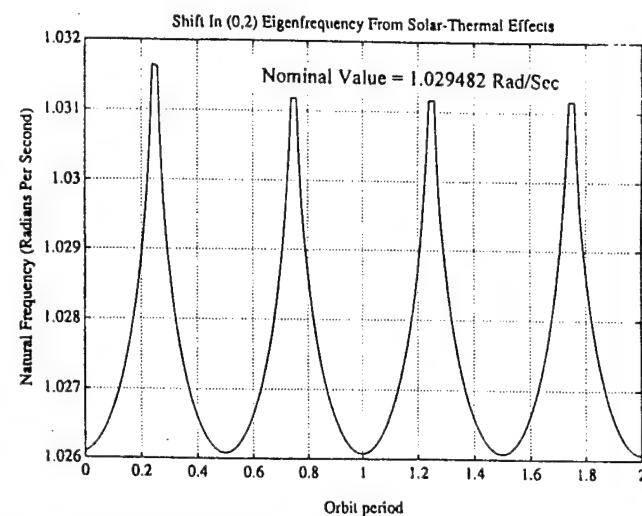
Fig. 20. Shell (0,2) Modal Frequency
Vs. Orbital Time
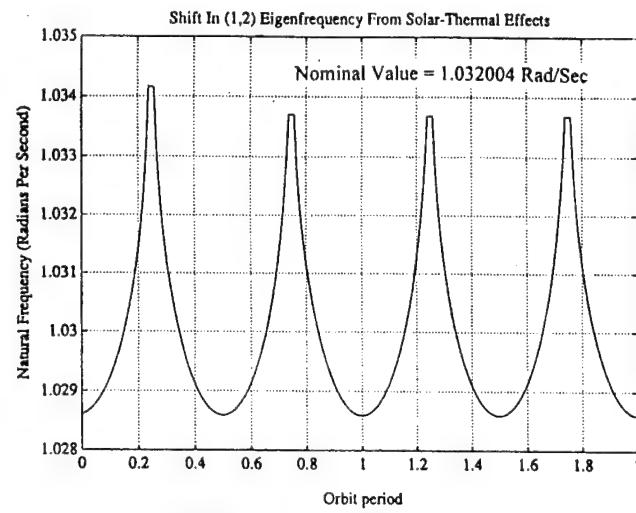
Fig.. 21. Shell (1,2) Modal Frequency
Vs. Orbital Time
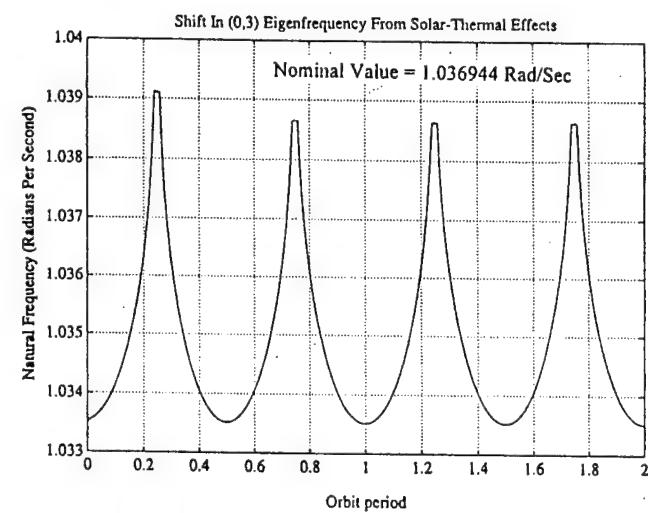
Fig. 22. Shell (0,3) Modal Frequency
Vs. Orbital Time
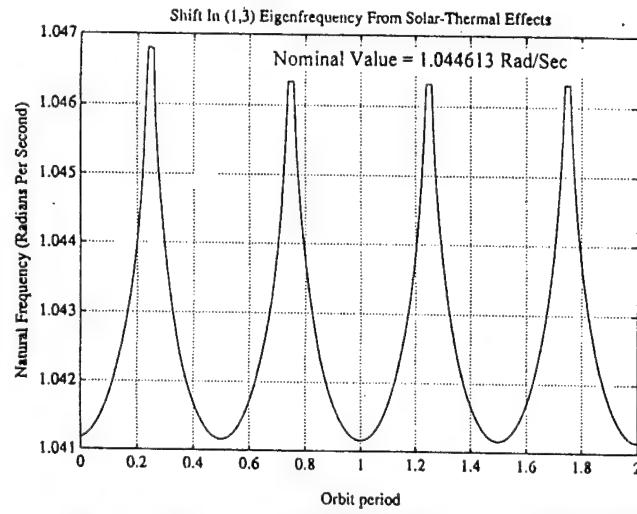
Fig. 23. Shell (1,3) Modal Frequency Vs. Orbital Time

2.15

III. LARGE-ANGLE NEAR-MINIMUM-TIME MANEUVER OF

RESHAPE WITH FLEXIBLE APPENDAGES

Abstract

In this chapter, we present our recent numerical and experimental results of the near-minimum-time maneuvers of the Naval Research Laboratory's Reconfigurable Spacecraft Host for Attitude and Pointing Experiments (RESHAPE) facility with flexible appendages. These maneuvers are designed as single axis maneuvers, but are tested on the three-dimensional testbed. The control strategy is based on the feedforward (open-loop solution) plus state-error feedback control. The open-loop solution is obtained by solving the so-called two-point boundary-value problem associated with the minimum-time maneuvers using a shooting method. This solution provides a bang-bang type control command for the prescribed reorientation requirements, i.e., to slew the structure from the known initial states to the final required attitude in a minimum-time sense. In the experiment, this open-loop control solution provides a "feedforward" control command and trajectories which the system is required to follow. The second loop, a state-error feedback control loop, is then designed to add guaranteed stability to the system, so that small disturbances during the maneuver and post-maneuver error can be damped out. The numerical and experimental results are presented to illustrate the success of this method.

3.1 Introduction

The objective of these maneuver tests is to achieve minimum-time or near-minimum-time maneuvers of a ground-based space structure with flexible appendages and, at the same time, to keep the vibration of the flexible components in a minimum. The Naval Research Laboratory's RESHAPE facility testbed is chosen for our test (refer to Refs. 1-4). The RESHAPE's configuration is shown in Fig. 1. The testing platform is supported by a spherical air bearing system and the platform can rotate freely about the pivot point, O, the center of the sphere. To achieve the objective, a pendulum is attached vertically by a string to the edge of the RESHAPE's circular platform to represent the flexible appendage. A sketch of the RESHAPE's coordinate system with the appendage is shown in Fig. 2. The rigid body system is then augmented by the two degrees of freedom of the pendulum motion under the restoring force induced by the gravity on the pendulum.

The first degree of freedom of the pendulum can be characterized by the swing angle, α, of the pendulum with respect to the vertical line through the hinge point, a. The second degree of freedom can be represented by the out of the tangential plane angular motion, i.e., by the angle between the projection line of the pendulum vector on the platform plane and the tangential plane, β, as shown in Fig. 2.

In this test, we consider only small amplitude flexible vibration motion, since we do not want to excite the flexible vibration too much. Under this consideration, the 3-dimensional (3-D) equations of motion of the system have been derived. It can be seen that the out-of-plane equation of motion is coupled with other equations through a coefficient $\sin\alpha$, where α is the angle of the pendulum with respect to the virtual line. Therefore, in the linearization process that follows, the out-of-plane motion is neglected. As a result we consider only the swing motion of the pendulum in the tangential plane which can be effectively considered as one flexible mode. In our tests, we mainly consider large-angle maneuvers about the yaw axis. The motion about the roll axis and the pitch axis are kept small. This reduces the control design to single-axis maneuver control of a rigid body with a single flexible mode. However, the test is still a 3-D test.

In the open-loop control design, a shooting method is used to solve the two-point boundary-value problem resulted from the Maximum principle for the maneuver problem. This solution provides a bang-bang type control command for the prescribed reorientation requirements, i.e., to slew the structure from the known initial states to the final required attitude in a minimum-time sense. In the experiment, this open-loop control solution provides a "feedforward" control command and trajectories which the system is required to follow. The second loop, a state-error feedback control loop, is then designed to add guaranteed stability to the system, so that small disturbances during the maneuver and post-maneuver error can be damped out.

3.2 System Equations

The 3-D dynamical equations of motion can be derived using Lagrange's approach. The kinetic energy of the system can be expressed as

$$T = T_M + T_h + T_m \tag{1}$$

where the subscripts M, h, and m refer to the platform, the reaction wheels, and the pendulum, respectively. Then,

$$T_M = \frac{1}{2}\omega^\top J_M \omega \tag{2}$$

where ω is the angular velocity vector and J_M is only the inertia matrix of the platform about the pivot point, O. Both ω and J_M are expressed in body axes (**i**, **j**, **k**). Next, by assuming that the rotation axes of the three reaction wheels are aligned orthogonally along the three body axes (**i**, **j**, **k**), respectively, we can obtain

$$T_h = \frac{1}{2} \sum_i \omega^T J_{h_i} \omega + \frac{1}{2} \sum_i J_i \Omega_i^2 + \sum_i J_i \Omega_i \omega_i \quad (i = 1, 2, 3) \tag{3}$$

where J_{hi} is the inertia matrix of the ith wheel with respect to the pivot point , O; J_i is the moment of inertia of the ith wheel about its rotation axis; and Ω_i is the relative angular rate of the ith wheel. The kinetic energy related to the pendulum can be obtained as

$$T_m = \frac{1}{2} m \left[\dot{L}^T \dot{L} + 2\omega^T (\tilde{R} + \tilde{L}) \dot{L} + \frac{1}{m} \omega^T J_m \omega \right] \tag{4}$$

where m is the mass of the pendulum, J_m is the inertia matrix of the pendulum with respect to O, and (referring Fig. 2)

$$R^T = [R_x \quad R_y \quad R_z], \quad R_x = R_1 \cos \beta_m, \quad R_y = R_1 \sin \beta_m$$

$$L = L_1 \begin{bmatrix} \sin\alpha \sin\bar{\beta} \\ \sin\alpha \cos\bar{\beta} \\ -\cos\alpha \end{bmatrix}, \quad \dot{L} = L_1 \begin{bmatrix} \dot{\alpha}\cos\alpha\sin\bar{\beta} + \dot{\beta}\sin\alpha\cos\bar{\beta} \\ \dot{\alpha}\cos\alpha\cos\bar{\beta} - \dot{\beta}\sin\alpha\sin\bar{\beta} \\ \dot{\alpha}\sin\alpha \end{bmatrix}$$

$$\bar{\beta} = \beta - \beta_m$$

where R_1 is the magnitude of the vector **R** projected onto the (**i**, **j**) plane of the RESHAPE coordinate system (Fig. 2). The "$\tilde{a}$" sign represents a 3x3 skew-symmetric matrix associated with a vector a,

$$\tilde{a} = \begin{bmatrix} 0 & -a_3 & a_2 \\ a_3 & 0 & -a_1 \\ -a_2 & a_1 & 0 \end{bmatrix}$$

3.3

The virtual work related to the gravity can be obtained as

$$\delta W_g = -\delta \theta^\top [(M+m_h)g\tilde{b} + mg(\tilde{R}+\tilde{L})]a_3 - mg(\delta \alpha L_\alpha^\top + \delta \beta L_\beta^\top)a_3 \tag{5}$$

where $\delta\theta$ is the virtual angle displacement vector, a_3 is the third column of the direction cosine matrix of the platform,

$$A = \begin{bmatrix} 2(q_0^2+q_1^2)-1 & 2(q_1q_2+q_0q_3) & 2(q_1q_3-q_0q_2) \\ 2(q_1q_2-q_0q_3) & 2(q_0^2+q_2^2)-1 & 2(q_2q_3+q_0q_1) \\ 2(q_1q_3+q_0q_2) & 2(q_2q_3-q_0q_1) & 2(q_0^2+q_3^2)-1 \end{bmatrix}$$

M is the mass of the platform, m_h is the mass of three wheels, b is the position vector from the pivot point to the center of mass of the system without the pendulum, g is the gravitational acceleration constant, and q is the attitude quaternion vector, $q^\top = [\ q_0\ q_1\ q_2\ q_3\ ]$.

We now can obtain Lagrange's equations for the quasi-coordinates related to ω, the rotational angles, φ, of the reaction wheels, and the pendulum swing angles, α and β,

$$(J_{M+h}+J_m)\dot{\omega}+J_d\dot{\Omega} + m(\tilde{R}+\tilde{L})\dot{L} = \tilde{\omega}\frac{\partial T}{\partial \omega}-m(\dot{\tilde{L}})\dot{L}-\dot{J}_m\omega+Q_\theta \tag{6}$$

$$J_d\dot{\Omega}+J_d\dot{\omega}=\tau_\varphi \tag{7}$$

where

$$J_d = \begin{bmatrix} J_1 & & \\ & J_2 & \\ & & J_3 \end{bmatrix}$$

3.4

τ_φ is the torque acting on the reaction wheels, J_{M+h} is the inertia matrix of the platform and the wheels together, and Q_θ is the generalized force vector. By substituting the generalized forces from Eq. (5) and Eq. (7) into Eq. (6), we can remove the term $\dot{\Omega}$,

$$(J_{M+h}+J_m-J_d)\,\dot{\omega}+m(\tilde{R}+\tilde{L})\ddot{L}$$

$$= u+\tilde{\omega}\frac{\partial T}{\partial\omega}-m(\dot{\tilde{L}})-\dot{J}_m\omega-[(M+m_h)g\tilde{b}+mg(\tilde{R}+\tilde{L})]a_3 \tag{8}$$

At the same time, we obtain the equations for α and β,

$$m[\ddot{L}^\top L_\alpha-L_\alpha^\top(\tilde{R}+\tilde{L})\dot{\omega}-2L_\alpha^\top\dot{\tilde{L}}\omega-\frac{1}{m}\omega\frac{\partial J_m}{\partial\alpha}\omega] \;=\; -mga_3^\top L_\alpha \tag{9}$$

$$m[\ddot{L}^\top L_\beta-L_\beta^\top(\tilde{R}+\tilde{L})\dot{\omega}-2L_\beta^\top\dot{\tilde{L}}\omega-\frac{1}{m}\omega\frac{\partial J_m}{\partial\beta}\omega] \;=\; -mga_3^\top L_\beta \tag{10}$$

$$L_\alpha = \begin{bmatrix} \cos\alpha\sin\bar{\beta} \\ \cos\alpha\cos\bar{\beta} \\ \sin\alpha \end{bmatrix}, \quad L_\beta = \begin{bmatrix} \sin\alpha\cos\bar{\beta} \\ -\sin\alpha\sin\bar{\beta} \\ 0 \end{bmatrix}$$

It can be proven that

$$\ddot{L} = \ddot{\alpha}L_\alpha+\ddot{\beta}L_\beta-(\dot{\alpha}^2 L-2\dot{\alpha}\dot{\beta}L_b+\dot{\beta}^2 L_a)$$

where

$$L_b = L_1\begin{bmatrix} \cos\alpha\cos\bar{\beta} \\ -\cos\alpha\sin\bar{\beta} \\ 0 \end{bmatrix}, \quad L_a = L_1\begin{bmatrix} \sin\alpha\sin\bar{\beta} \\ \sin\alpha\cos\bar{\beta} \\ 0 \end{bmatrix}$$

It can be seen here that for small angle α and β,

$$\cos\alpha \approx 1, \quad \cos\bar{\beta} = \cos(\beta - \beta_m) \approx \cos\beta_m$$

$$\sin\alpha \approx \alpha, \quad \sin\bar{\beta} = \sin(\beta - \beta_m) \approx -\sin\beta_m$$

the β motion Eq. (10) is coupled with ω motion Eq. (8) and α motion Eq. (9) by a small quantity $\sin\alpha$. Therefore, for our present small α amplitude analysis, we drop Eq. (10) from further consideration.

For the purpose of simulation, we need to obtain the linearized equation of the system. In addition to small α and β, we also assume small q_1, q_2, ω_1 and ω_2. As a result, all second and higher order terms related to α, β, q_1, q_2, ω_1, and ω_2 are neglected,

$$J_T\dot{\omega} + m\begin{bmatrix} lc \\ ls \\ L_1R_1 \end{bmatrix}\ddot{\alpha} = u + \omega_3\begin{bmatrix} -J_{12}\omega_1 + (J_{33} - J_{22})\omega_2 + J_{23}\omega_3 \\ (J_{11} - J_{33})\omega_1 + J_{12}\omega_2 + J_{13}\omega_3 \\ J_{23}\omega_1 - J_{13}\omega_2 \end{bmatrix} + \begin{bmatrix} J_3\omega_2\Omega_3 - J_2\omega_3\Omega_2 \\ J_1\omega_3\Omega_1 - J_3\omega_1\Omega_3 \\ J_2\omega_1\Omega_2 - J_1\omega_2\Omega_1 \end{bmatrix}$$

$$-(M+m_h)g\begin{bmatrix} b_2 - 2b_3(q_2q_3 + q_0q_1) \\ 2b_3(q_1q_3 - q_0q_2) - b_1 \\ 2b_1(q_2q_3 + q_0q_1) - 2b_2(q_1q_3 - q_0q_2) \end{bmatrix} - mg\begin{bmatrix} R_y + \alpha c + 2l(q_2q_3 + q_0q_1) \\ 2l(q_0q_2 - q_1q_3) - R_x + \alpha s \\ 2R_x(q_2q_3 + q_0q_1) - 2R_y(q_1q_3 - q_0q_2) \end{bmatrix} \quad (11)$$

$$mL_1^2\ddot{\alpha} + m[\,lc \quad ls \quad L_1R_1\,]\dot{\omega} = 2m\,\omega_3 l(c\omega_2 - s\omega_1) - mg[2c(q_2q_3 + q_0q_1) - 2s(q_1q_3 - q_0q_2) + L_1\alpha] \quad (12)$$

Note that these are linear equations for α, β, q_1, q_2, ω_1, and ω_2 only. J_{ij} is the element of the constant inertia matrix J_T,

$$J_T = J_{M+h} + \bar{J}_m - J_d$$

where

$$\bar{J}_m = m \begin{bmatrix} R_y^2+l^2 & -R_x R_y & R_x l \\ -R_x R_y & R_x^2+l^2 & R_y l \\ R_x l & R_y l & R_1^2 \end{bmatrix}$$

and

$$l = L_1 - R_z, \quad c = L_1\cos\beta_m, \quad s = L_1\sin\beta_m$$

To further simplify the analysis, we can neglect the terms related to the gravity, the body rates, and the rates of the wheels in the ω equation, and the terms related to the body rates and quaternions in the α equation,

$$J_T\dot{\omega} + m \begin{bmatrix} lc \\ ls \\ L_1 R_1 \end{bmatrix} \dot{\alpha} = u \tag{13}$$

$$mL_1^2\ddot{\alpha} + m[lc \quad ls \quad L_1 R_1]\dot{\omega} = -mgL_1\alpha \tag{14}$$

The 2-dimensional (2-D) equations involving only ω_3 and α can be obtained immediately as,

$$mR_1 L_1\dot{\omega}_3 + mL_1^2\ddot{\alpha} = -mgL_1\alpha \tag{15}$$

$$(J_{(M+h)_s} - J_{h_s} + mR_1^2)\dot{\omega}_3 + mL_1 R_1\ddot{\alpha} = u_3 \tag{16}$$

3.3 Time Optimal Control of the 2-D System and 3-D Feedback Control

The time optimal control for the 2-D system can be obtained by using the maximum principle. The formulation of the time-optimal control is based on the following cost functional

$$J = \int_0^{t_f} dt = t_f$$

The Hamiltonian of the system can be formed by introducing costates and the necessary conditions for the optimal control can be derived. The control is of bang-bang type and can be obtained numerically by solving the associated two-point boundary-value problem. The shooting method from Ref. 2 is used for solving the nonsingular TPBVP.

The solution of the optimal control of the 2-D system is used as the open-loop control or feedforward control of the 3-D system. This solution includes the quaternion, $q(t)$, angular velocity, $\omega(t)$, and control, $u(t)$. The solution for $\alpha(t)$ is not considered in the feedback control loop. The errors between these computed values and the measured values ("real") of these variables are

$$\delta q = q_m - q(t), \quad \delta\omega = \omega_m - \omega(t)$$

where ω_m is obtained from the output of the rate gyros, and q_m is obtained from integration of the kinematic equations using Euler's first order integration method. These errors, the error quaternion, δq, and error angular velocity, $\delta\omega$, are used in the state-error feedback control loop to obtain the correction control, δu,

$$\delta u_i = -k_p \delta q_{i+1} - k_r \omega_i, \quad i = 1, 2, 3.$$

where k_p and k_p are constants. The resulting control signal is the combination of the open-loop control and the feedback control,

$$u(t, \delta q, \delta\omega) = u(t) + \delta u$$

It is clear that the torque constraints for the open loop control (bang-bang type) should be set below the maximum allowable level of the physical system, so that some leeway can be left for the correction control. As a rule of thumb, we can use 80~90% of the allowable control for the open-loop control design and 10~20% for the correction control. This results in the near-minimum-time maneuvers under the allowable control constraints.

3.8

3.4 System Parameters

The description of the RESHAPE facility can be found from Ref. 1. The RESHAPE structural parameters used in the simulations are listed below:

Inertial matrix of the RESHAPE without the pendulum:

$$J_{M+h} = \begin{bmatrix} 14.42 & .15 & .28 \\ .15 & 17.85 & .42 \\ .28 & .42 & 27.82 \end{bmatrix} \ (ft\text{-}lb\text{-}sec^2)$$

Momentum of inertia of the reaction wheels: $J_1 = J_2 = J_3 = .054$ (ft-lb-sec^2);
Gravitational constant: $g = 32.174$ (ft/sec^2);
RESHAPE weight = 638.0 (lb);
Angle between the position vector of the pendulum hinge point and body i axis: $\beta = \pi/2$;
Length of the position vector of the pendulum hinge point: $R_1 = 2.5$ (ft);
z-coordinate of the position vector of the pendulum: $R_z = 0.0$;
Length of the pendulum: $L_1 = 4.5$ (ft);
Pendulum weight: $mg = 5.0$ (lb);
Position vector of the RESHAPE without the pendulum: $b_1 = 0.0$; $b_2 = -mR_1/(M + m_h)$; $b_3 = 0.0$;

Sampling Time: 0.05 sec;
Feedback control gains: k_p = [24.8846 30.2138 49.7636], k_r = [44.22 53.69 88.43];
Maximum control torque for the open-loop control u_3 : $u_{3max} = 0.4$ (ft-lb);
Extra control effort for the feedback control are:
$\delta u_3 = 0.001056 \sim 0.08976$ (ft-lb), depending on the cases;
Extra control for the other two axes (pitch and roll) are: $\delta u_2 = \delta u_1 = 0.5 \delta u_3$.

3.5 2-D Optimal Control Solution and 3-D Simulation

The 2-D dynamic equations (15) and (16) are used to find the time-optimal control solution. This is a single-axis maneuver of a rigid body with a flexible mode. We here consider only the rest-to-rest maneuvers and the associated boundary conditions of the state variables are chosen as

$$\alpha(0) = 0, \quad \dot{\alpha}(0) = 0, \quad \omega_3(0) = 0, \quad \theta_3(0) = \theta_{30};$$

$$\alpha(t_f) = 0, \quad \dot{\alpha}(t_f) = 0, \quad \omega_3(t_f) = 0, \quad \theta_3(t_f) = 0.$$

For the RESHAPE system with parameters described in section 3.4, we have obtained maneuver solutions from $\theta_{30} = 1$ deg to $\theta_{30} = 180$ deg. Two typical maneuver solutions, 25 deg and 180 deg maneuvers, are shown in Fig. 3 and Fig. 4, respectively. The time-optimal controls for these maneuvers are of bang-bang type and three intermediate switches are required. The minimum time for the 25 deg maneuver is 11.312 sec and three intermediate switches are separated by 0.6 sec. The minimum time for the 180 deg maneuver is 30.091 sec and the time interval between the three intermediate switches is 0.6 sec. The occurrence of triple switches is clearly associated with the addition of the flexible mode included into the system compared with the purely single-axis maneuver of a rigid body. The well-known result for the latter case is a single switch in the middle of the slewing period. It is shown that the pendulum angle and pendulum rate are very small for this particular RESHAPE system setup. This small amplitude vibration is also observed during the hardware test.

We have observed, through computations, that the time interval between the triple switches is different from case to case, depending on the system parameters and initial conditions. If all other parameters are fixed and only the initial condition, θ_{30}, is changed from 1 deg to 180 deg, the time interval between the three switches changes periodically. At some particular values of θ_{30}, we are able to obtain a zero interval. This means a single switch case where all the three switches are collapsed together, even though there is a flexible mode involved here. But these are only a few isolated cases and an elaborate analysis will not be conducted in this report. Except these isolated points, all other cases result in triple switches. We choose the 25 deg maneuver because the triple switches in this case are well separated, and choose the 180 deg case because it can be considered as the "largest" angle rotation for the rest-to-rest maneuvers.

The solution for these maneuvers is usually not available in analytical form compared with the classical single-axis rigid body maneuver, and therefore, can not be generated at run-time. However, we are interested in finding out the advantage of applying this solution to the maneuver test over using the single switch solution. Before we go to the test, let us look at results of the 3-D simulations for these two open-loop control commands. The results for the triple switch and the single switch results are presented in Figs. 5, and 6 for the 25 deg maneuver case, respectively. The single switch command for the latter method is obtained as if there is no flexible part. By comparing these two figures, we can see that using the triple switch command will reduce the vibration of the pendulum both during the second half of the maneuver and post maneuver. This in return will reduce the attitude errors and rates. The pendulum angle and rate are also shown in Figs. 5 and 6. The testing results for this comparison will be discussed later.

We should point out that we use both control command feedforward as well as state trajectory feedforward in our control strategy. This is quite different from using only the command feedforward method. Actually, we can observe this by examining Fig. 5 and Fig. 6. Before the first switch near 5 sec., both control commands (open-loop) are the same $u_3 = -0.4$ ft-lb. But the 3-D responses of the control, u_3 are different. Also the δq_3 in these two figures are different. This is because the feedforward trajectories for these two method are different, as shown in Fig. 7.

3.10

The time responses of the reaction wheels for the triple switch simulation, φ and Ω are also shown in Fig. 7 for the case $\delta u=0.03696$. Other cases are similar. The nonzero values for Ω are due to the gravitational torque terms presented in Eq. (11). This phenomenon is also observed during the test, where the reaction wheels for the x and y axes keep running after the maneuver. If the values of α or q are not zero, there will be some gravitational torques on the platform which balance the torques from the reaction wheels. Even though the torques applied to the wheels are zero, other parameters or factors may also lead to the nonzero momentum accumulation of the wheels during the maneuver. Further analysis is needed on this subject.

3.6 3-D Test Results and Numerical Simulations

Using the feedforward and state-error feedback method described in section 3.3, we have conducted the hardware tests and 3-D numerical simulations. Five tests for the 25 deg maneuver are presented here as shown in Figs. 8-11. The first four tests are using the triple switch solution and the fifth test is using the single switch method for the comparison purpose. For the triple switch maneuvers, we have used four different extra control effort levels, δu_3, for the feedback control use as discussed in section 3.3. These values are 0.001056, 0.01056, 0.03696, 0.08976 (ft-lb) for the four cases, about 0.2% to 22% of the open-loop control saturation level, 0.4 (ft-lb). Also shown in Figs. 8-11 are the 3-D simulations using the 3-D equations (7), (11), and (12).

From Figs. 8-11, as the extra control effort is increased, the errors of q_3 are reduced and the overshoot of ω_3 at the end of the maneuver is also reduced. The errors for q_1, q_2, ω_1, and ω_2 do not change significantly. We also see that there is no similarity between testing results and simulation results for errors of q_1, q_2, w_1, w_3, u_1, and u_2. Further analysis needs to be done in this area. We also see that the control history of the simulation is close to the open-loop control command (not shown), while the control signal from the test deviates more from the open-loop solution either for the smaller leeway case, Fig. 8c, or the larger leeway case, Fig. 11c. We believe that the overshoot of the control at the end of the maneuver is due to the inaccuracy of the inertial term and the difference in the inertial terms between the 2-D and 3-D representing models of the system.

In Fig. 12, we put the triple switch case and single switch results together for comparison. We observe that the triple switch method results in less residual vibration, even when the error magnitudes are the same. This indicates the advantage of using the triple switch solution especially for the well-separated time interval between the three middle switches.

The test for 180 deg maneuver are presented here in Figs. 13-15. Three different levels of δu_3 are considered. Again, either small leeway or large leeway results in large deviation of the control from the bang-bang type. The case, $\delta u_3=0.03696$ (ft-lb, about 9.2% of 0.4 ft-lb), in Fig. 14 seems to be the closest one to the bang-bang type control of the open-loop solution. It is also seen that the errors in the quaternion during the maneuver are reduced as more control freedom is allowed.

3.11

Another problem with the 180 deg maneuver is that the triple switches presented in the simulations do not occur in the test. The reason for this needs to be found out. One reason might be that the 180 deg maneuver requires longer slewing time than the 25 deg maneuver. The "mid" point or middle region is "relatively" small compared with the whole slewing time and is, therefore, not significant for the feedback control adjustment.

3.7 Conclusions

A practical control strategy for the minimum-time maneuver problem has been developed and successfully applied to the RESHAPE hardware test facility. The open-loop time-optimal control provides a basis for the nonlinear large-angle near-minimum-time maneuver, while the linear feedback control takes care of disturbances during the maneuver and damps out the residual vibration after the maneuver. This is the first time that the bang-bang type and feedback control strategy has been applied to the RESHAPE hardware testing facility with flexible appendages.

An extensive optimal control solution for the 2-D system has been obtained. 3-D simulations by using both triple and single switch methods have been conducted. Use of the triple switch command will reduce the vibration of the pendulum and the attitude errors both during the second half of the maneuver and post maneuver. As the extra control effort is increased, the state errors are reduced. An adequate level of the extra control leeway seems to be about 10% of the open-loop control saturation level so that the control will be close to the bang-bang type, the maneuver will be near minimum-time, and less post maneuver vibration and state errors will result.

The success of the test is demonstrated by the excellent correlation between numerical simulations and experimental testing results. This test demonstrates the applicability and the effectiveness of this simple feedforward and state-error feedback control strategy. This technique can be easily transferred to other types of three-axis, nonlinear, and time-optimal maneuver experiments or actual tests.

Further analysis needs to be done in the areas such as the identification of the isolated single switching point, the reduction of the terminal angular rates of the reaction wheels, the determination of the reason for the non-similarity of the state errors between the test and the simulations, and the reason for the disappearance of the triple switches in the test for the 180 deg maneuver case. Improvements and extensions of the control strategy to three-axis slewings and vibration suppression of the rigid platform containing other flexible appendages or antennas are recommended.

References

3.1   CREAMER, N.G. and TENEZA, N.C. "RESHAPE: An Experimental Facility for Satellite Control," *Proceedings of the American Control Conference*, Chicago, IL, June 24-26, 1992, pp. 2001-2005.

3.2   "RESHAPE: A Laboratory for Research in Satellite Attitude Control and Control/Structures Interaction," Naval Research Laboratory Report, Washington, D.C., 1992.

3.3   Li, F., Bainum, P.M., Creamer, N.G., Fisher, S., and Teneza, N.C., "Three-Axis Near-Minimum-Time Maneuvers of RESHAPE: Numerical and Experimental Results," presented at the *AIAA/AAS Space Flight Mechanics Meeting*, Cocoa Beach, Florida, February 14-16, 1994, AAS Paper 94-154, accepted for publication in **The Journal of the Astronautical Sciences**.

3.4   Li, F., Bainum, P.M., Creamer, N.G, Fisher, S., and Teneza, N.C., "RESHAPE Experiments for Near-Minimum-Time Feedback Maneuvers," presented at the *19th International Symposium on Space Technology and Science*, Yokohama, Japan, May 15-24, 1994.
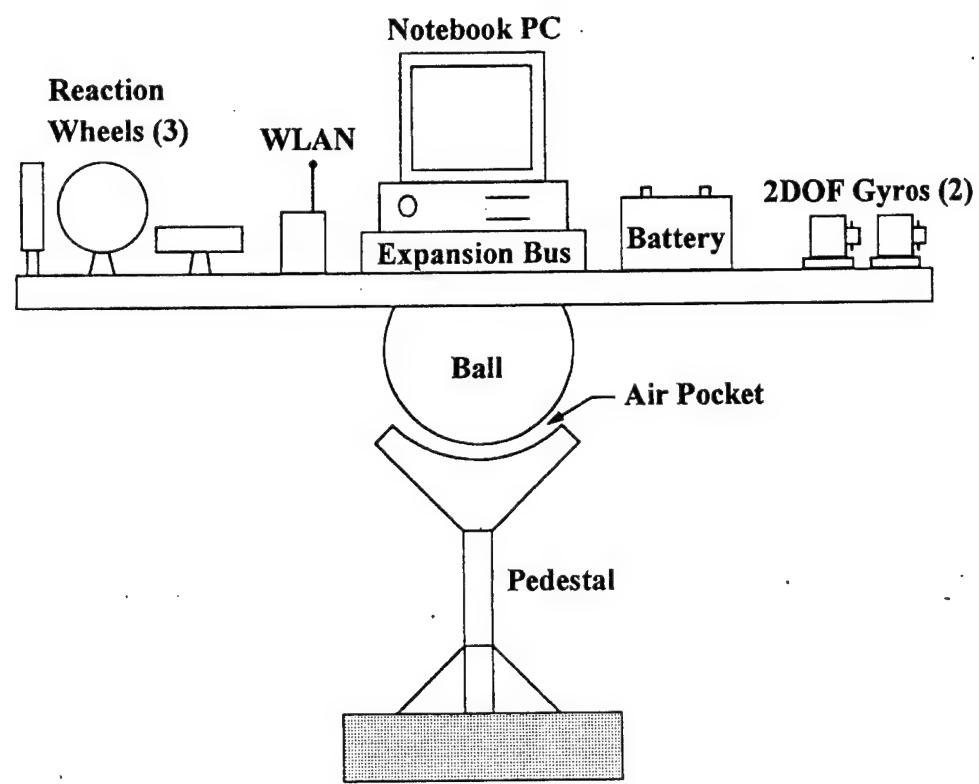
Fig. 1 Configuration of the RESHAPE Facility, NRL
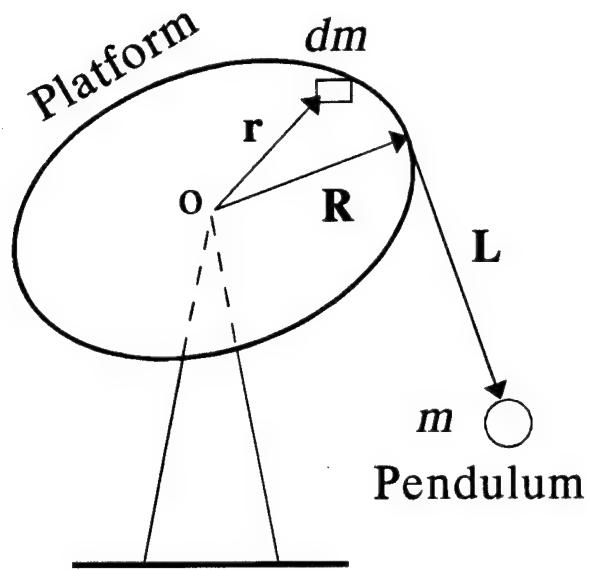
(a) Vector Notations.
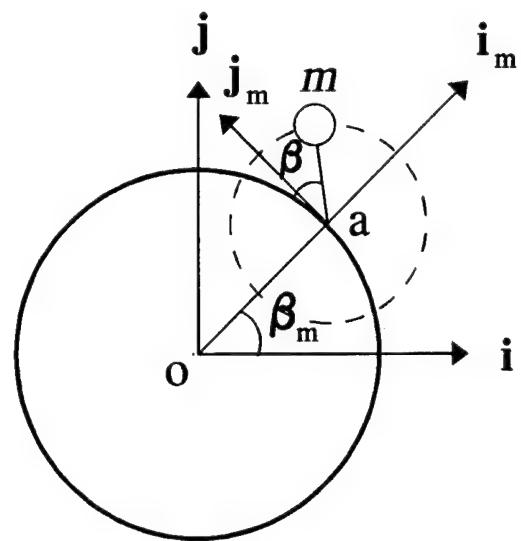
(b) Top View.
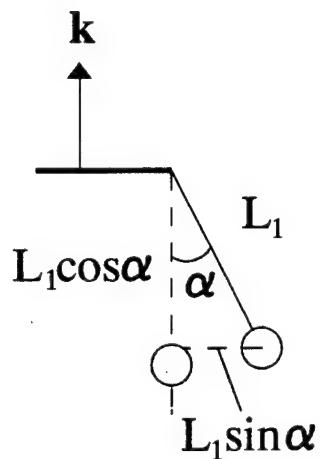
(c) Side View.

Fig. 2 RESHAPE Coordinate System.
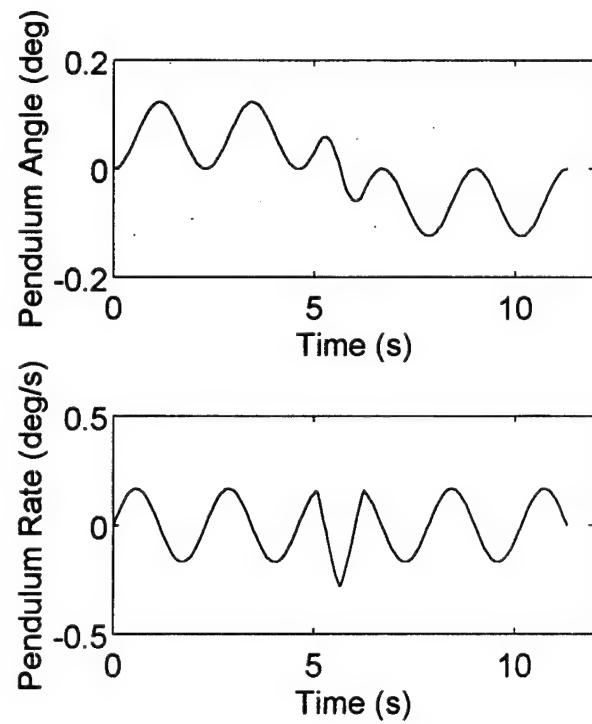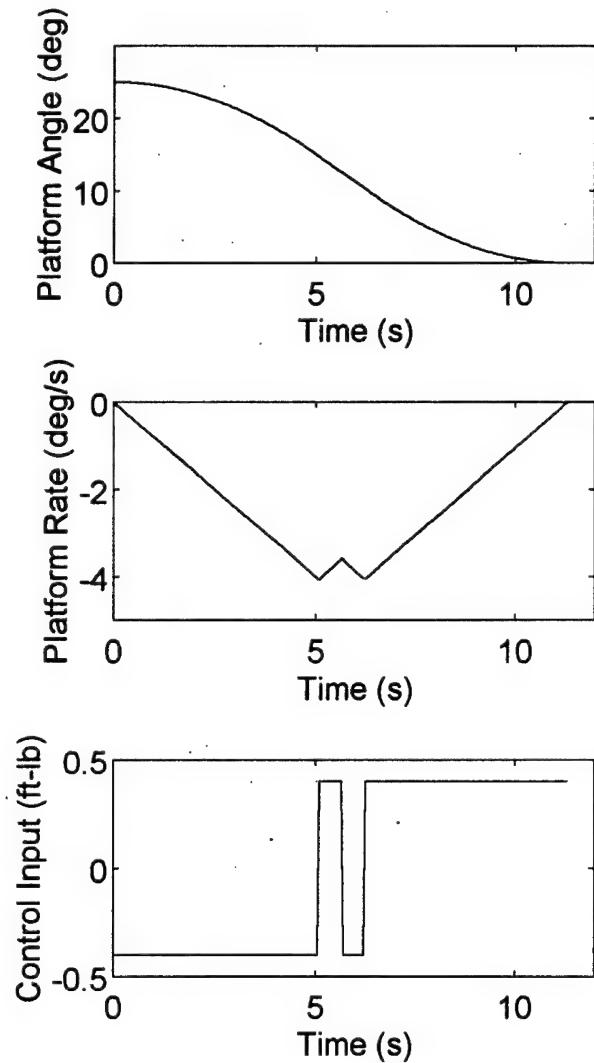
Fig. 3

2-D RESHAPE Optimal Slew:

Yaw Axis Torque u3max=0.4 ft-lb,

Slew Angle=25 deg.
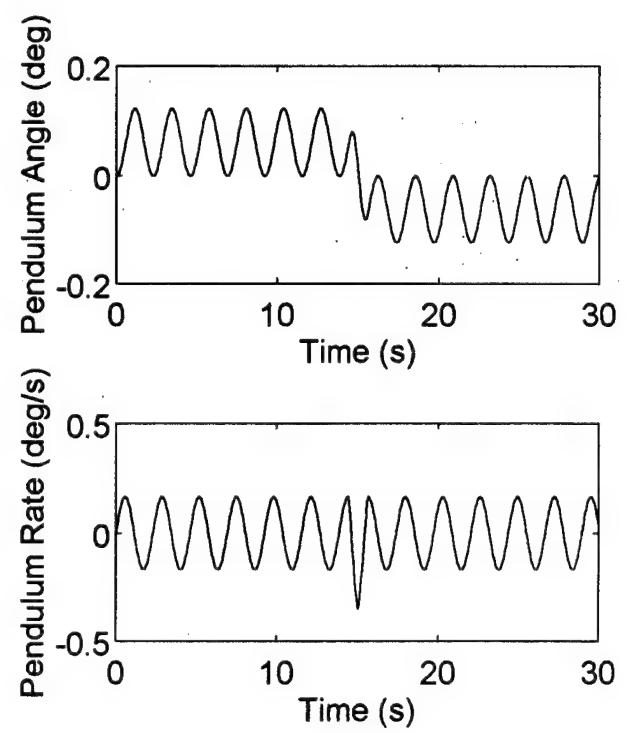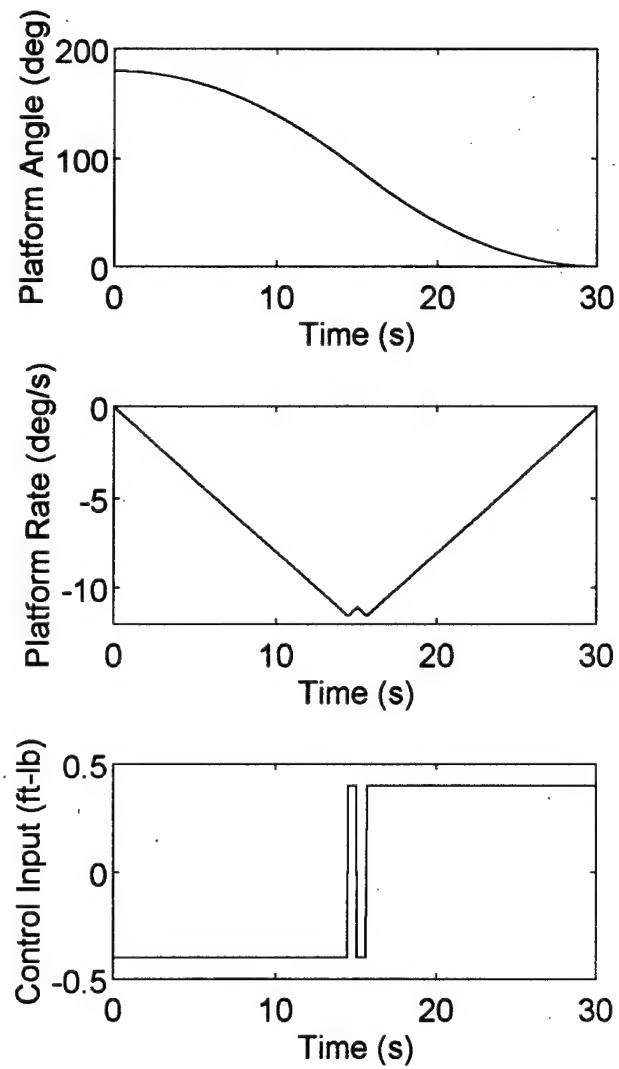
Fig. 4

2-D RESHAPE Optimal Slew:
Yaw Axis Torque u3max=0.4 ft-lb,

Slew Angle=180 deg.

3.17
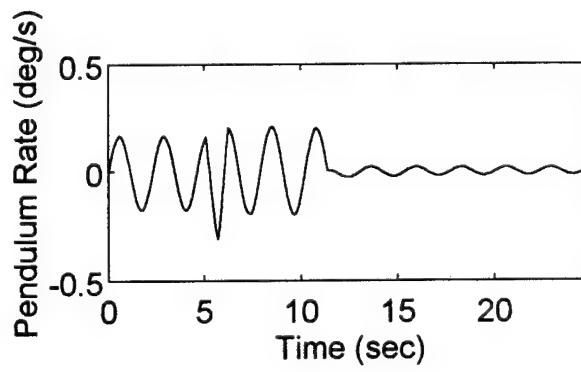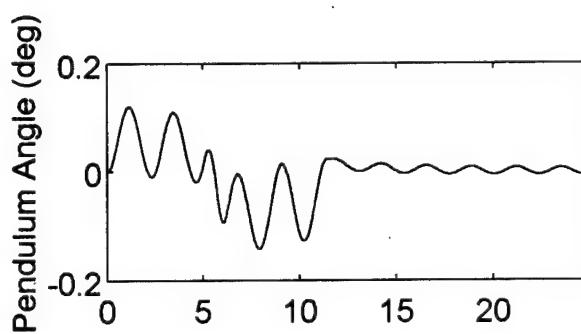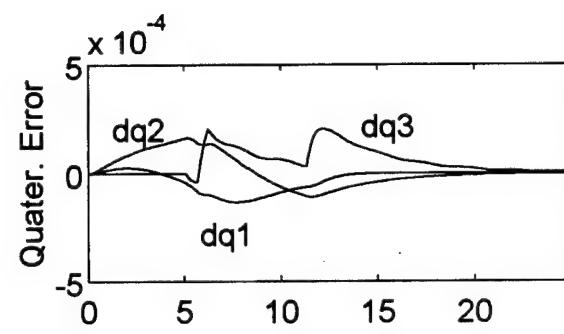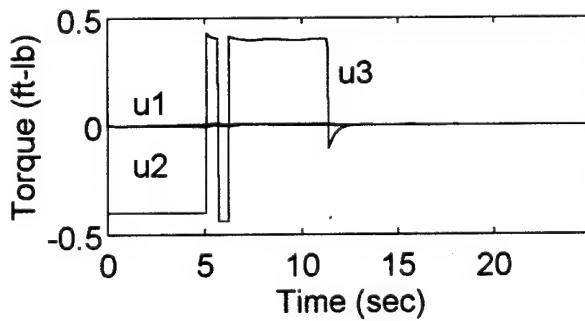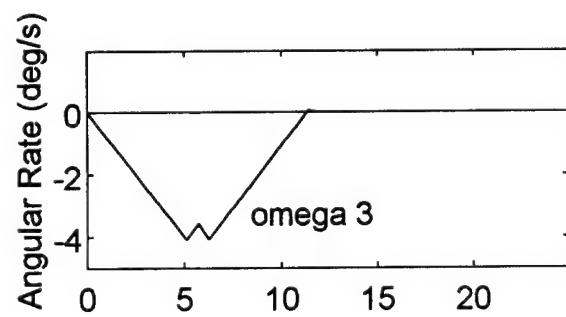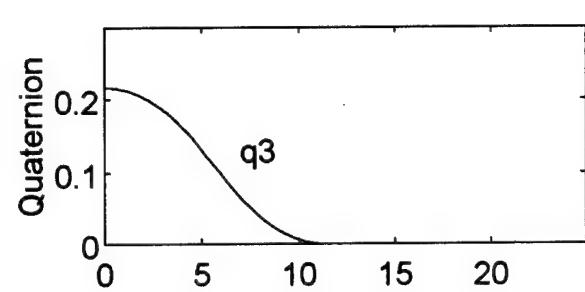
Fig. 5   3-D Maneuver Simulation: Triple Switch Case, 25 deg, du3=0.03696 ft-lb.

3.18
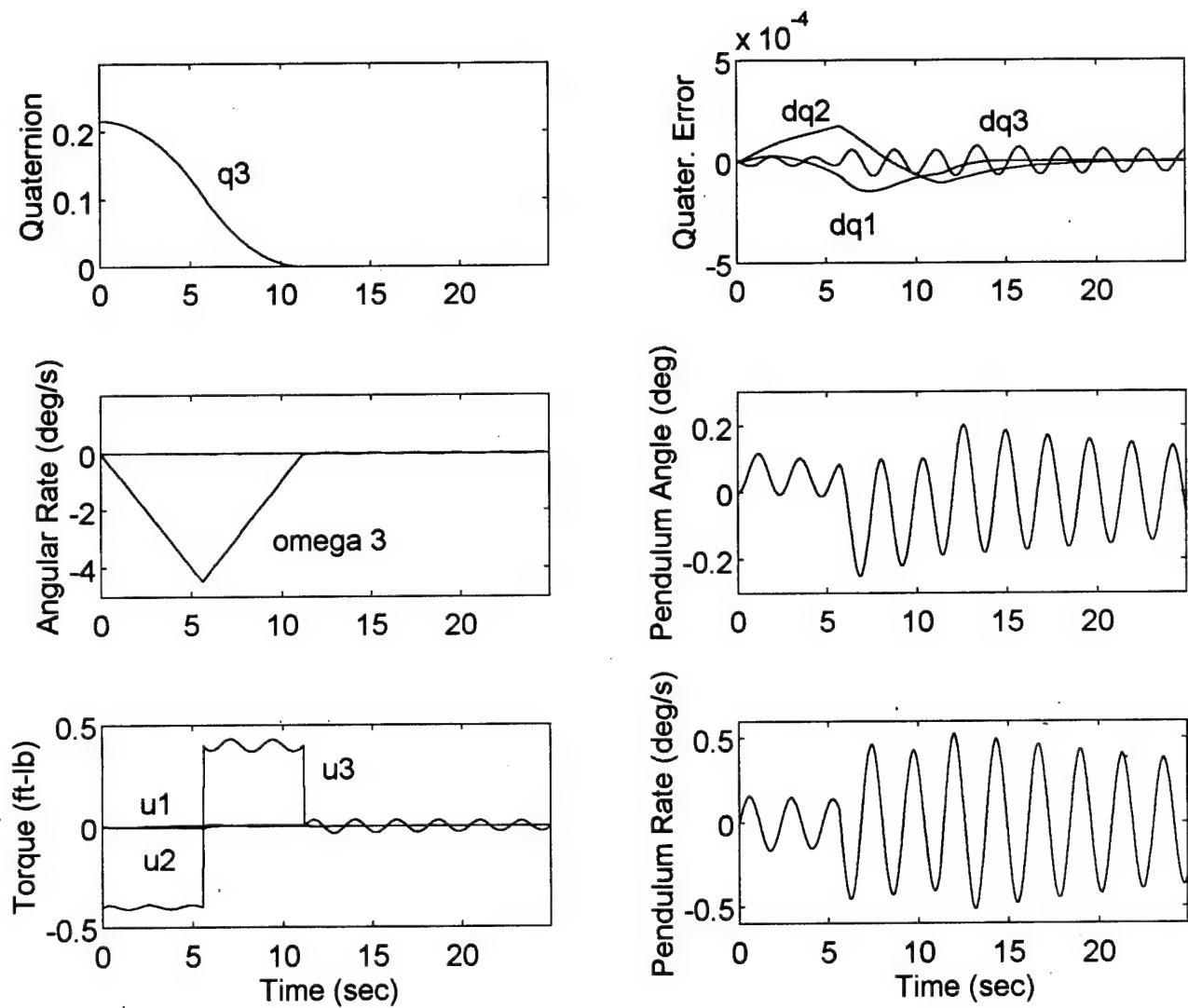
Fig. 6   3-D Maneuver Simulation: Single Switch Case, 25 deg, du3=0.03696 ft-lb.

3.19
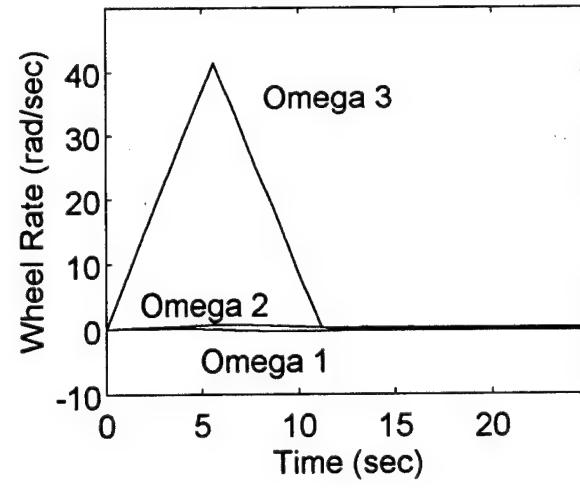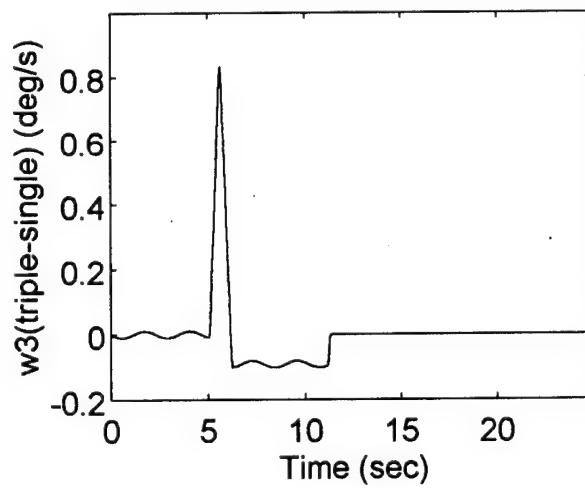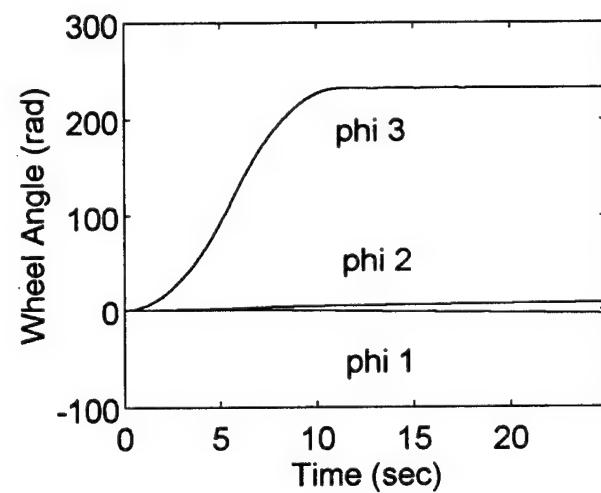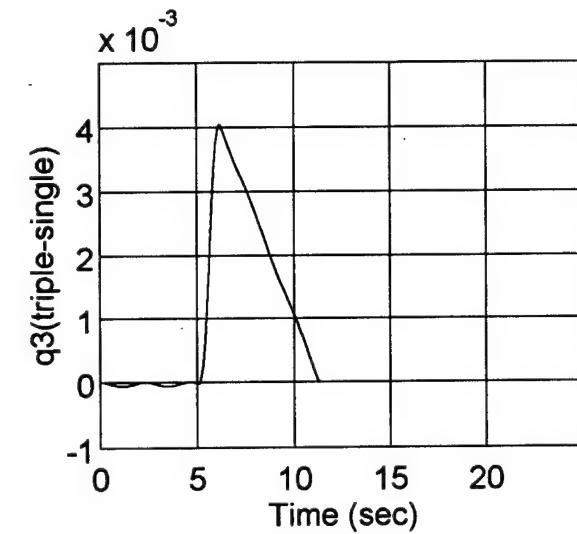
Fig. 7   3-D Maneuver Simulation: 25 deg, du3=0.03696 ft-lb:
Feedforward Trajectory Difference between the Triple and Single Switch Cases;
Reaction Wheel Responses for the Triple Switch Case.

3.20
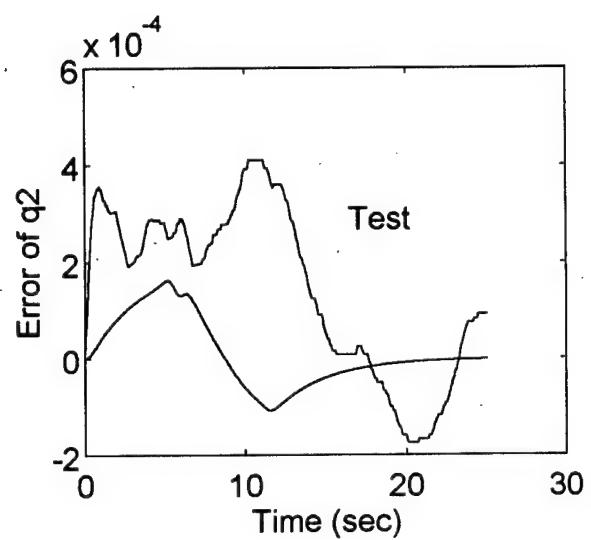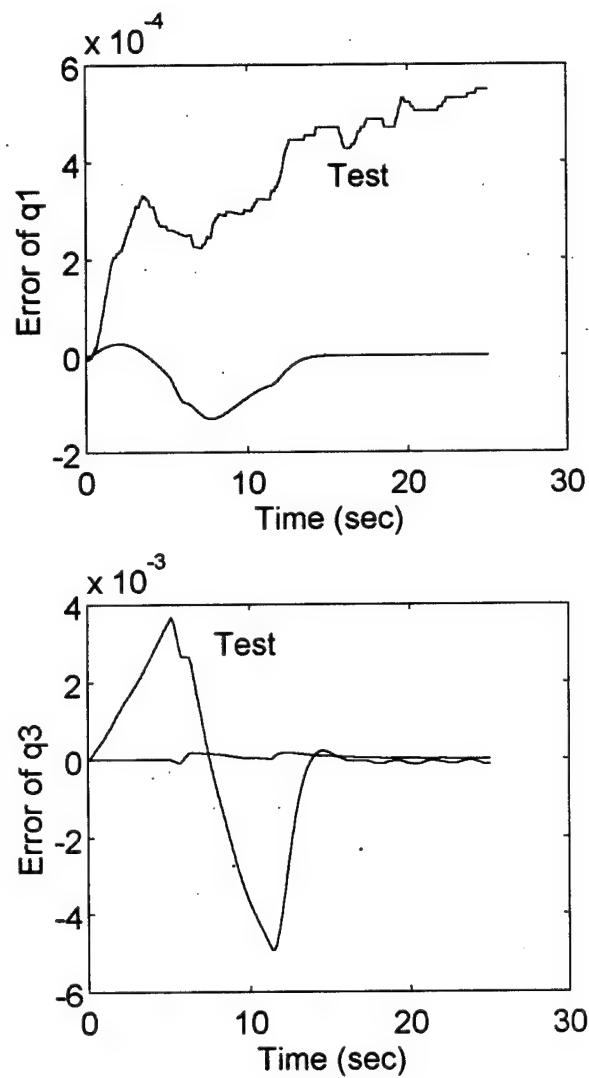
Fig. 8a
RESHAPE Maneuver:
25 deg Simulation and Test
du=0.001056 ft-lb
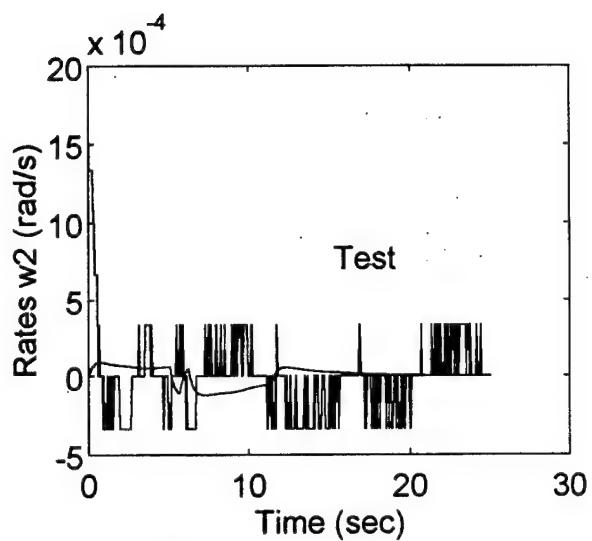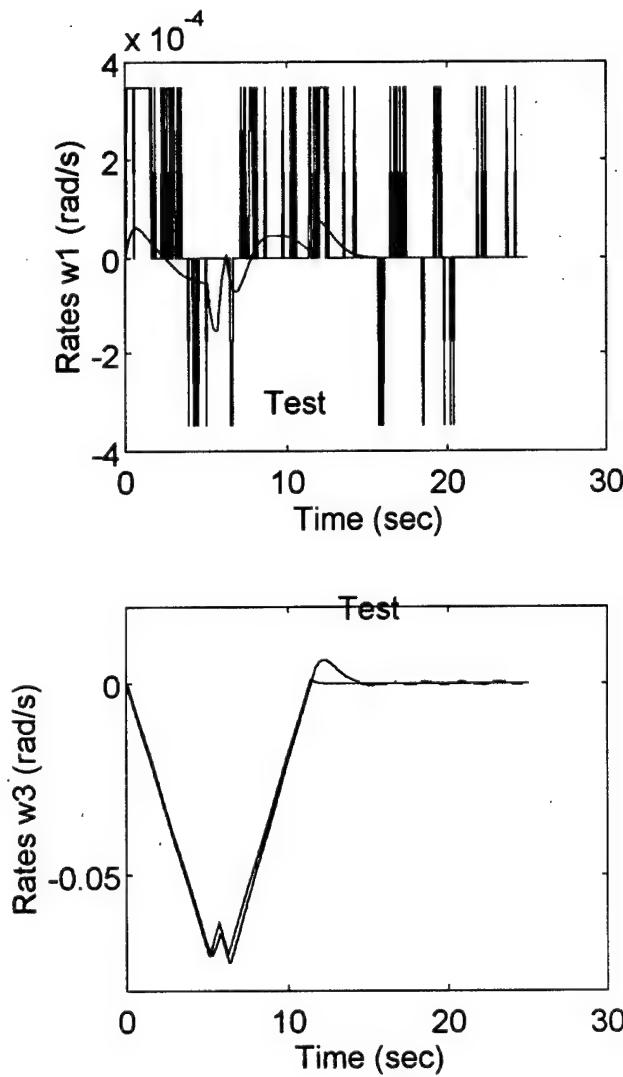
Fig. 8b

RESHAPE Maneuver:

25 deg Simulation and Test

du=0.001056 ft-lb

3.22
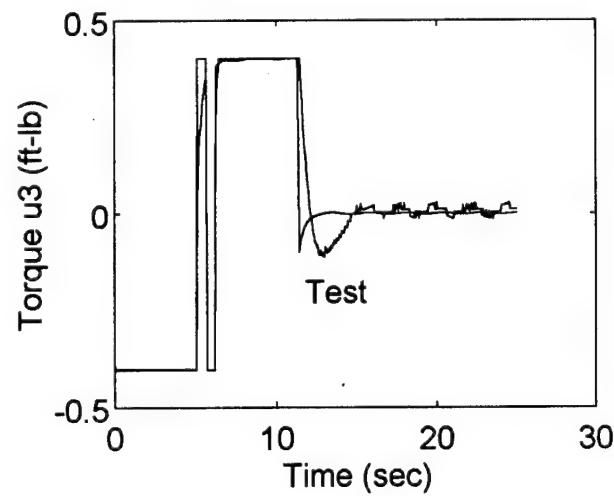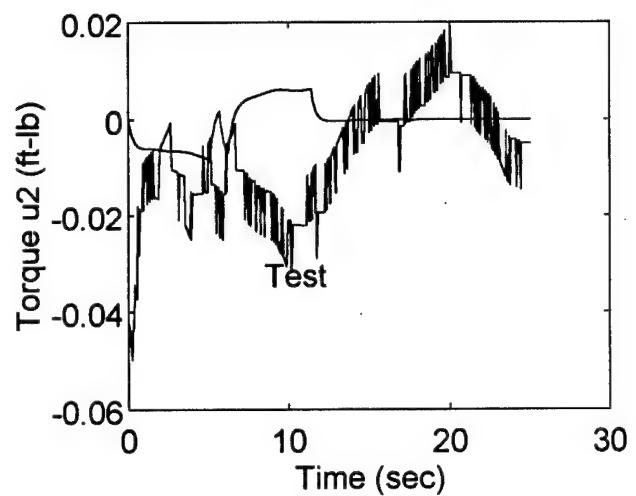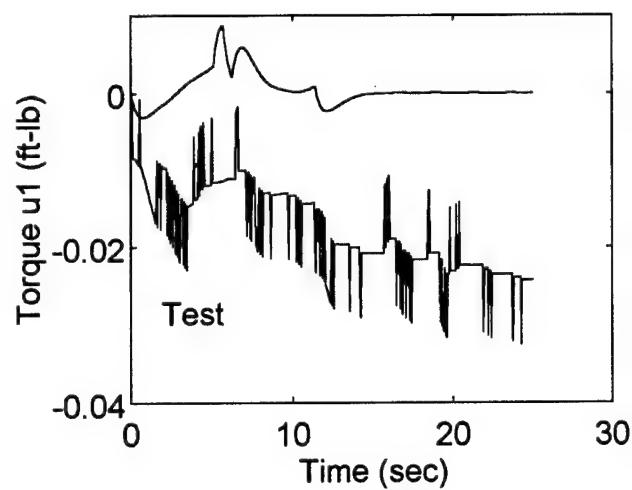
Fig. 8c
RESHAPE Maneuver:

25 deg Simulation and Test
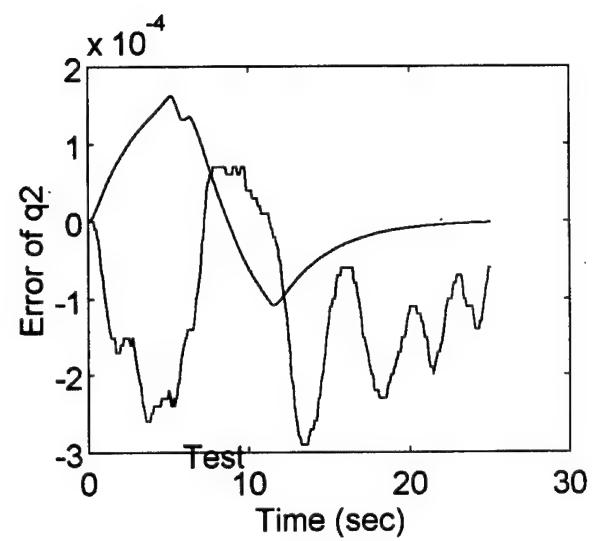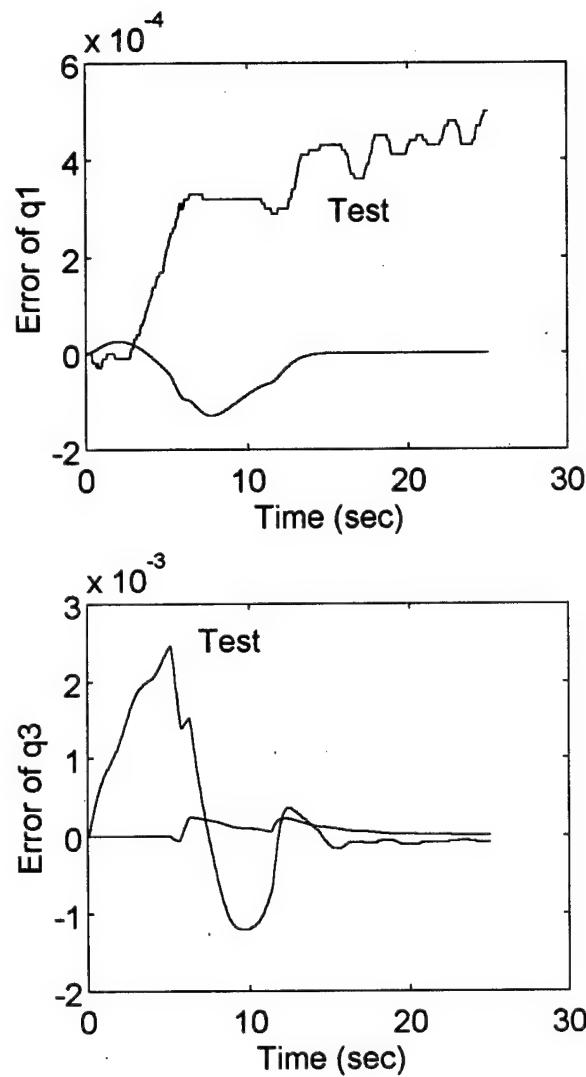
du=0.001056 ft-lb

Fig. 9a

RESHAPE Maneuver:

25 deg Simulation and Test

du=0.01056 ft-lb

Fig. 9b

RESHAPE Maneuver:

25 deg Simulation and Test

du=0.01056 ft-lb

3.25
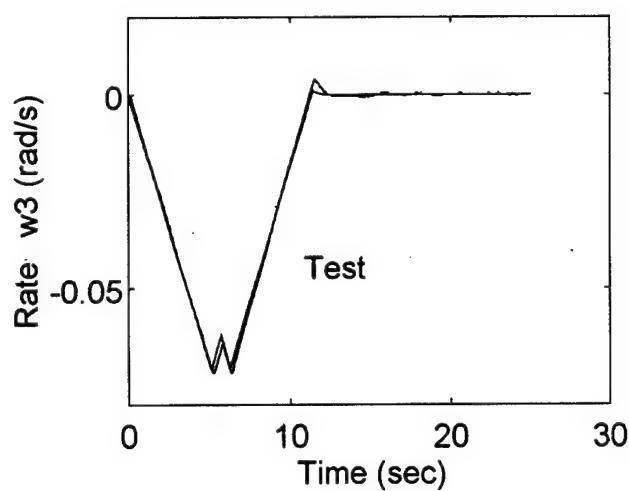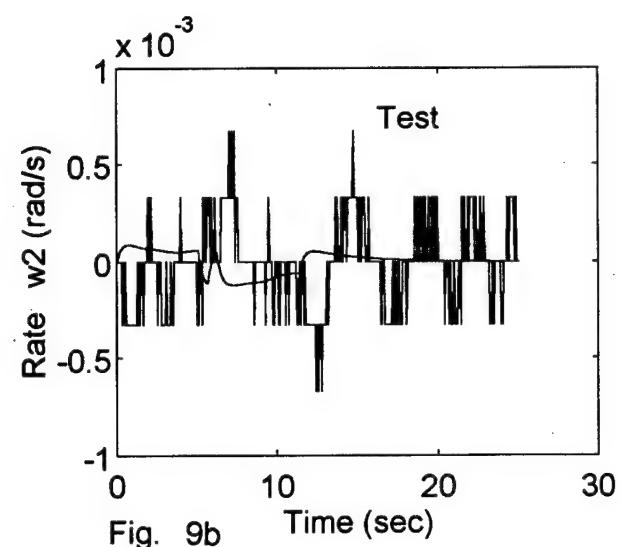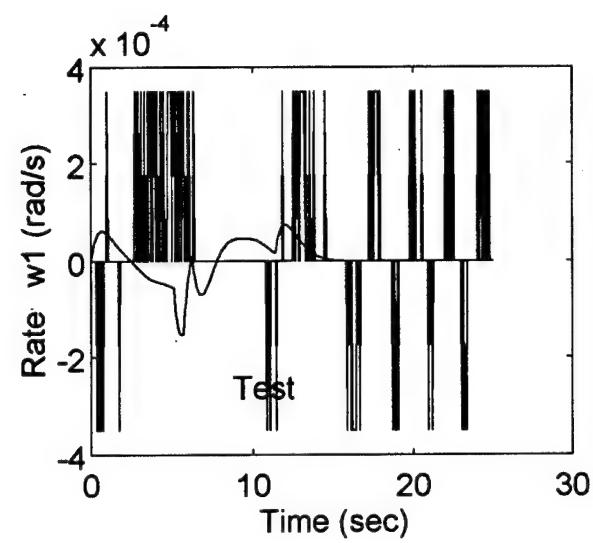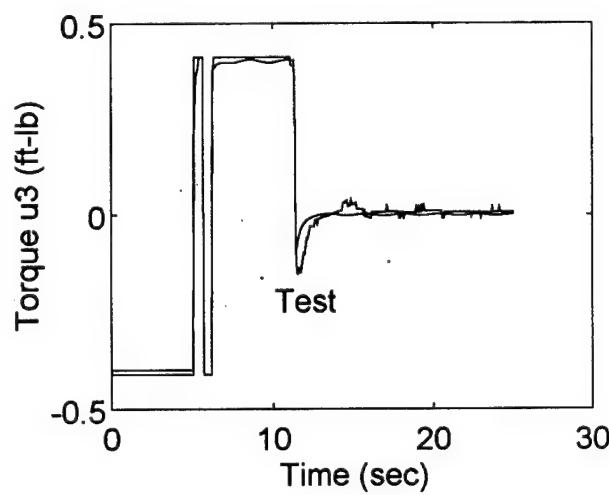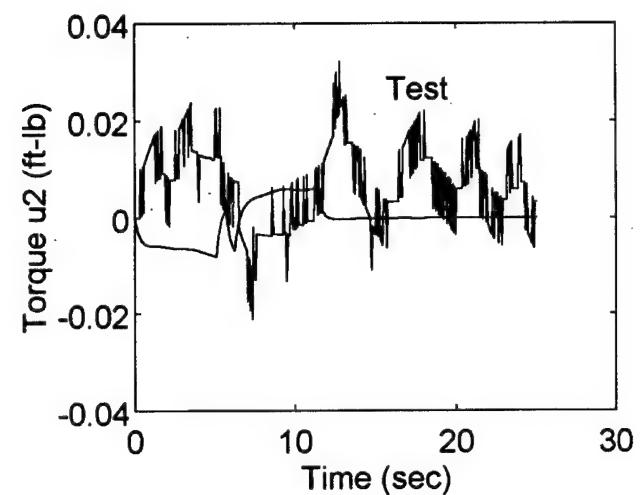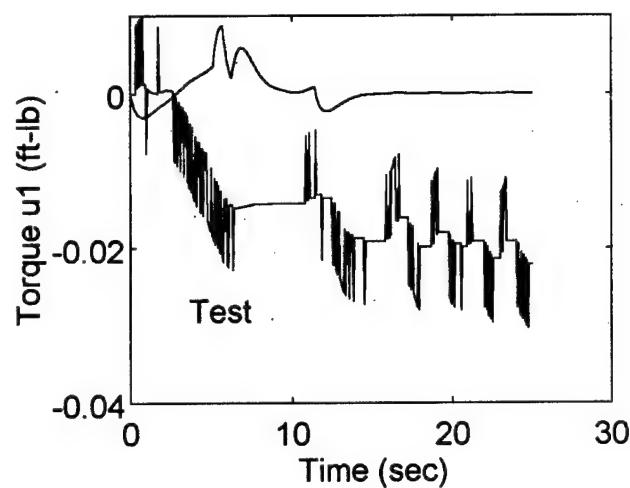
Fig. 9c

RESHAPE Maneuver:

25 deg Simulation and Test

du=0.01056 ft-lb

Fig. 10a
RESHAPE Maneuver:
25 deg Simulation and Test
du=0.03696 ft-lb
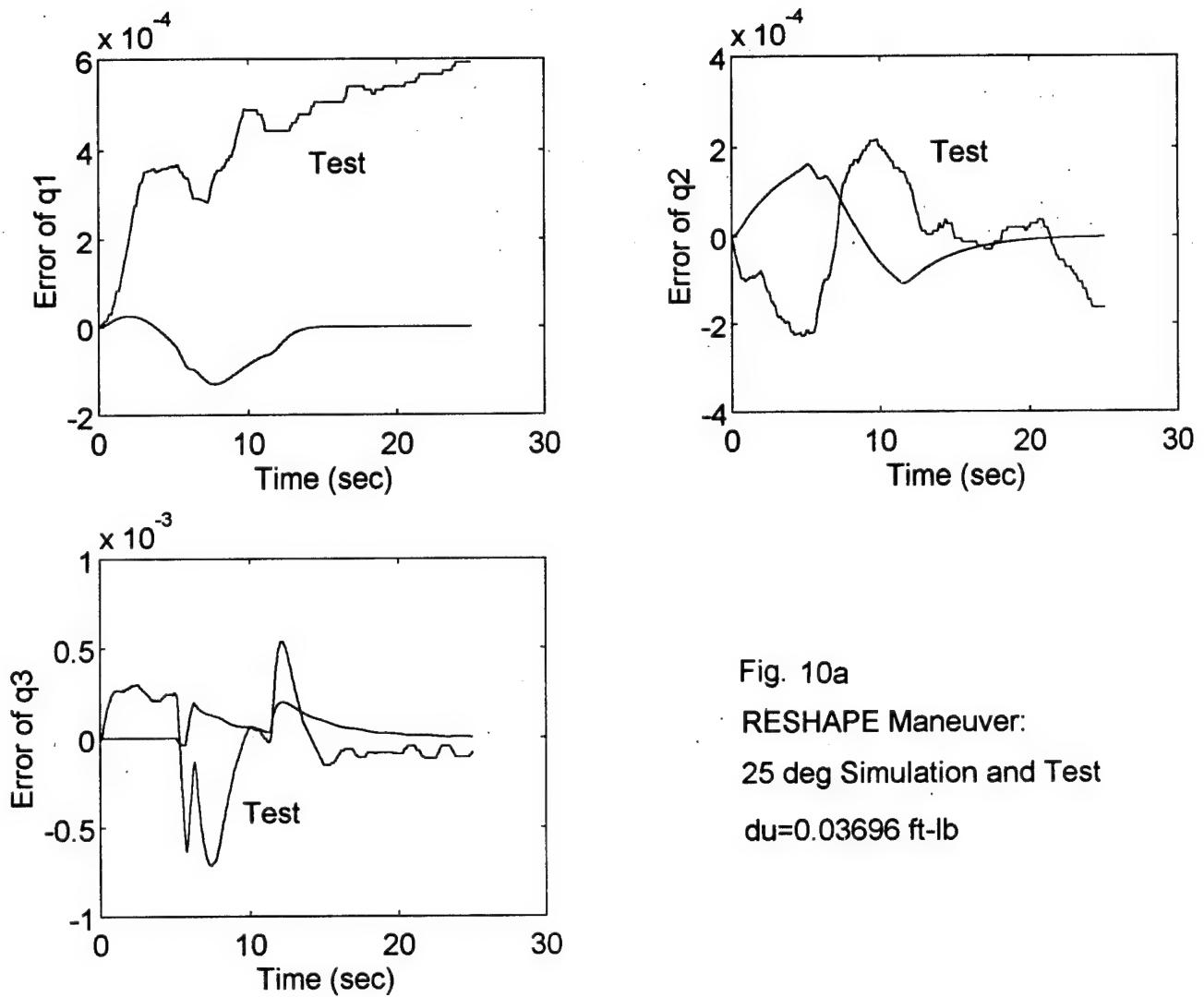
Fig. 10b

RESHAPE Maneuver:

25 deg Simulation and Test
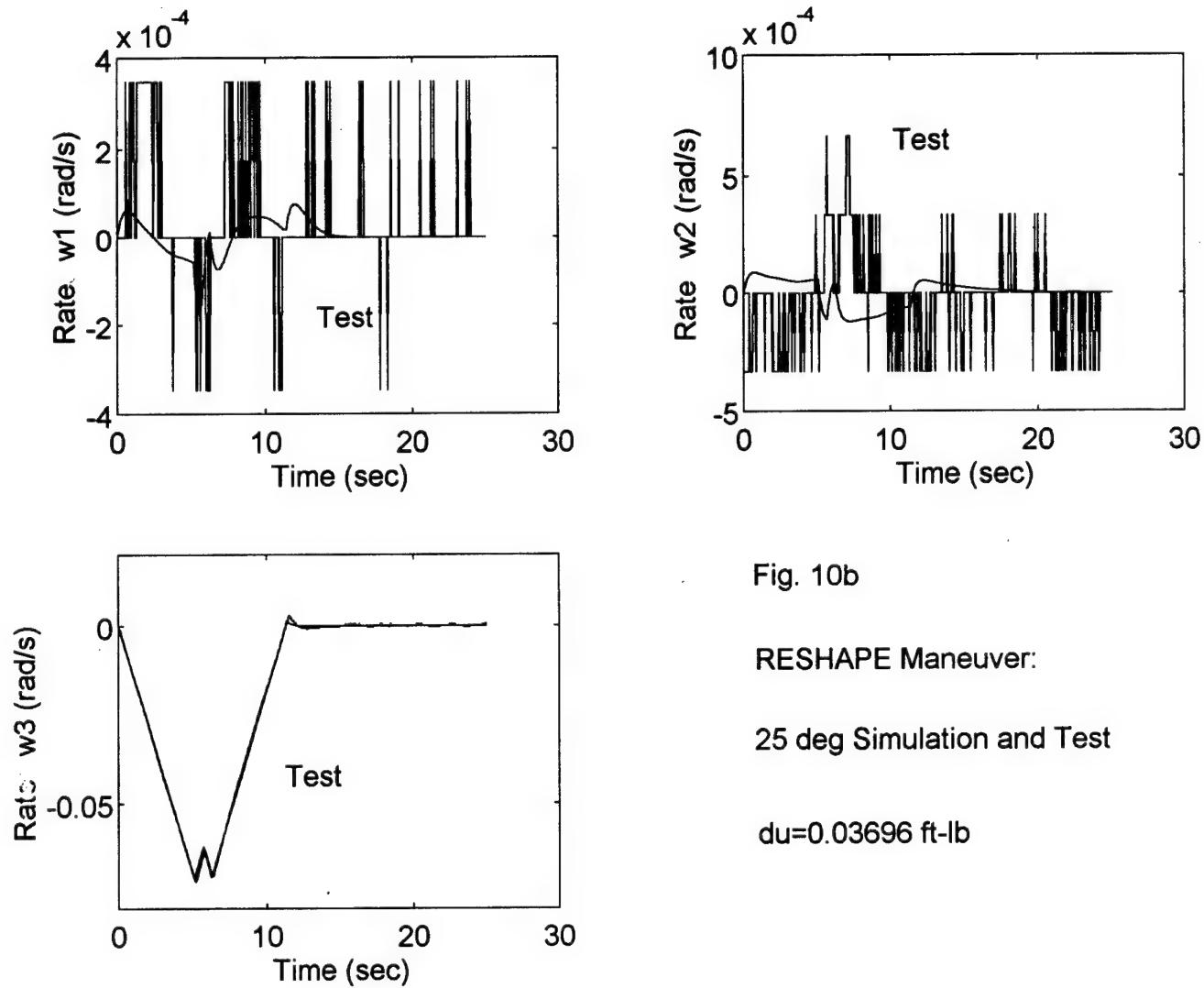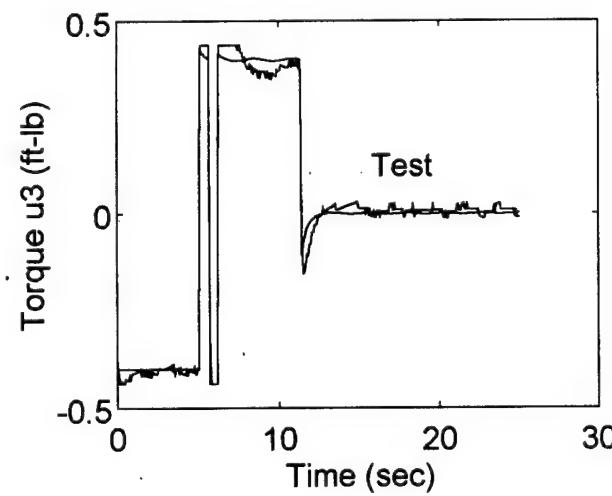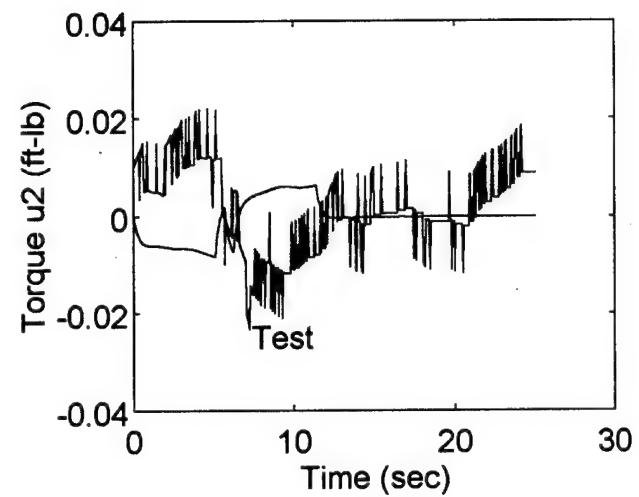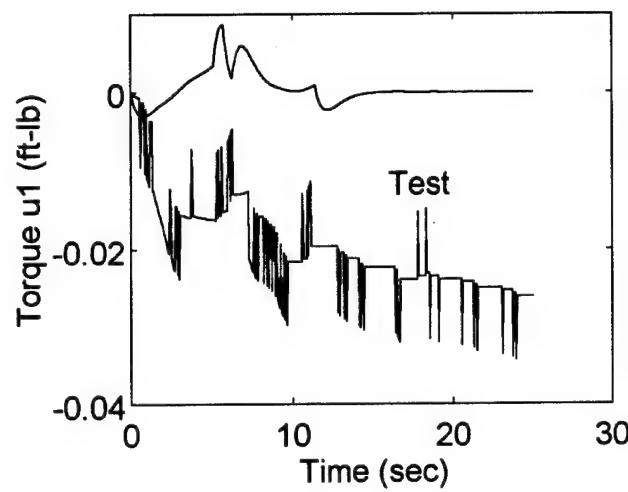
du=0.03696 ft-lb

Fig. 10c
RESHAPE Maneuver:
25 deg Simulation and Test
du=0.03696 ft-lb
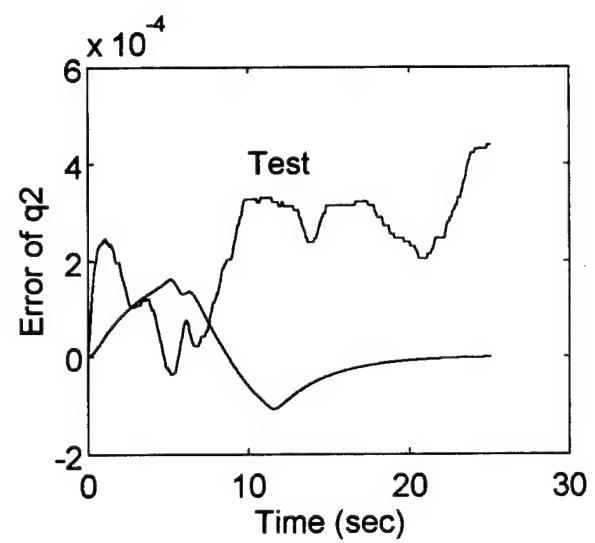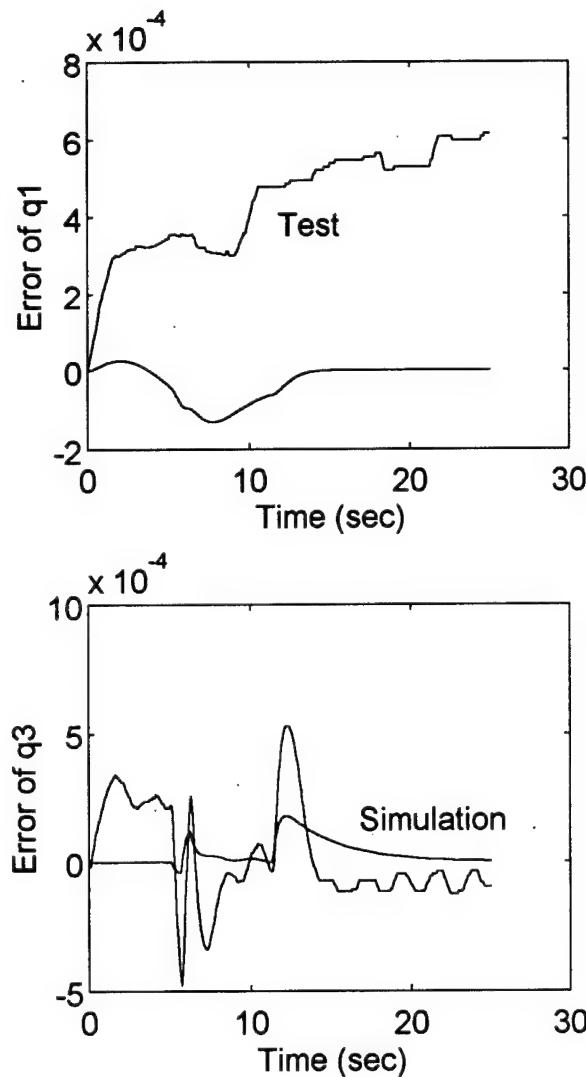
Fig. 11a
RESHAPE Maneuver:
25 deg Simulation and Test
du=0.08976 ft-lb

Fig. 11b

RESHAPE Maneuver:

25 deg Simulation and Test

du=0.08976 ft-lb

3.31
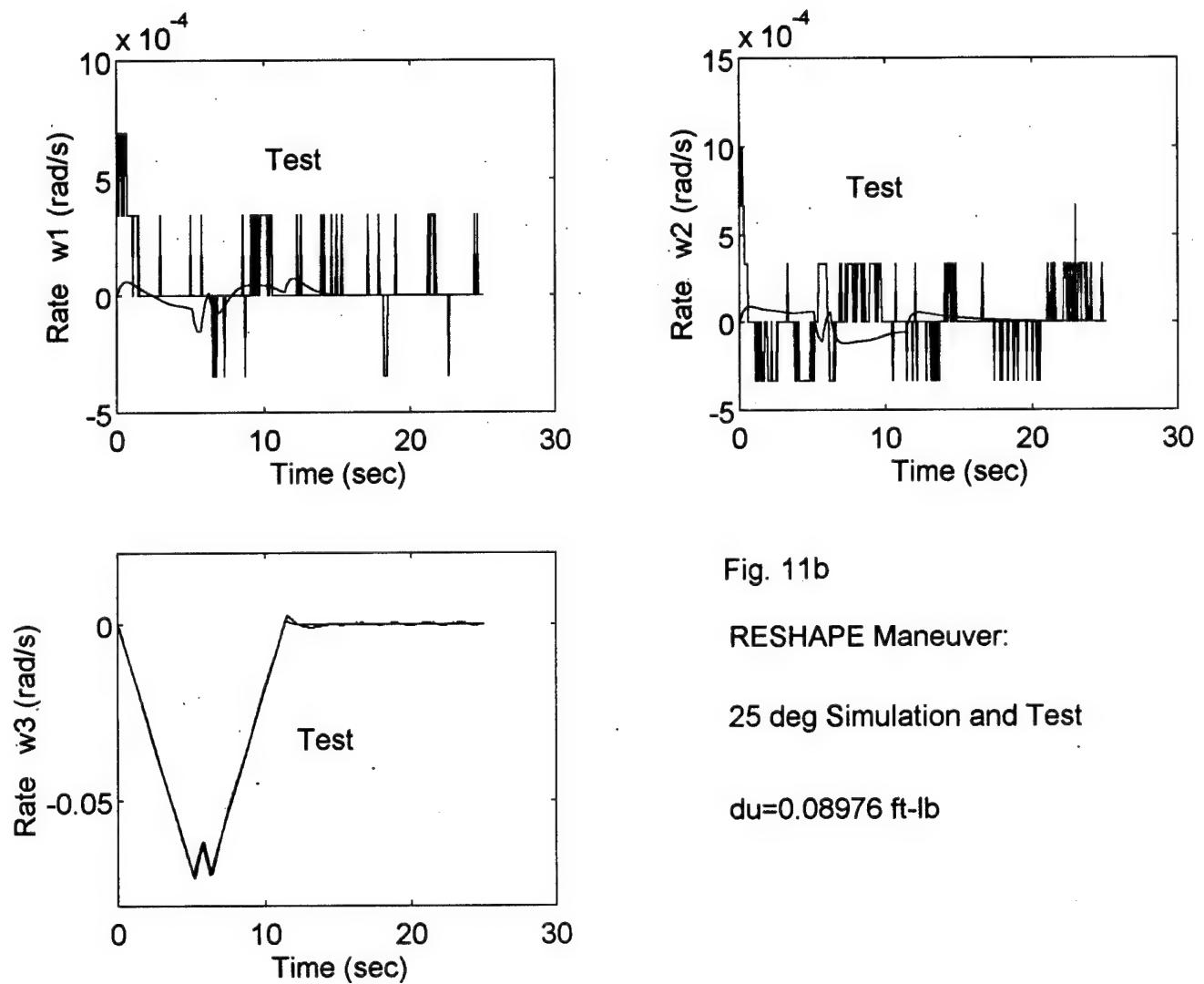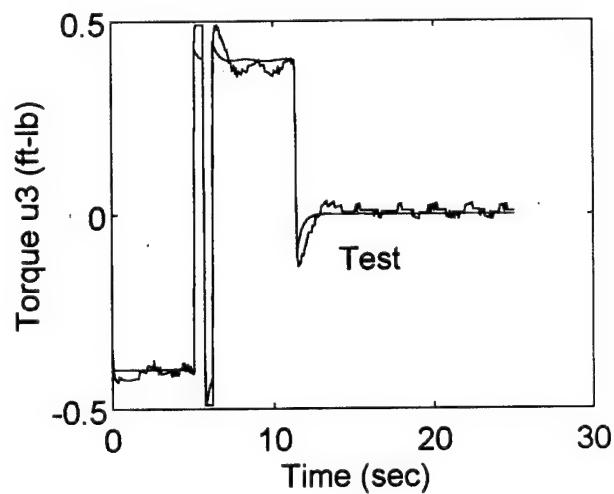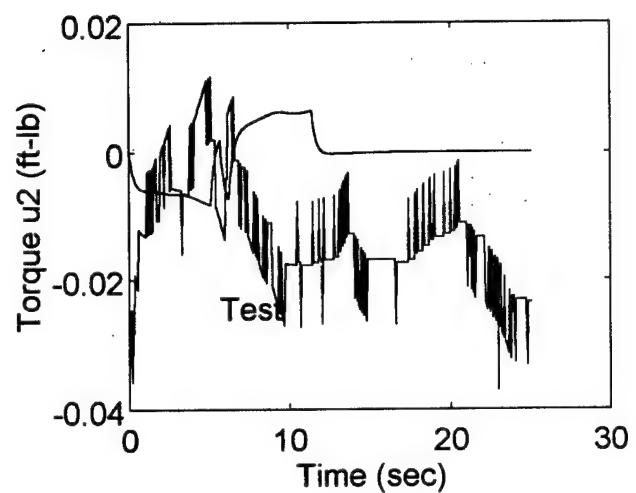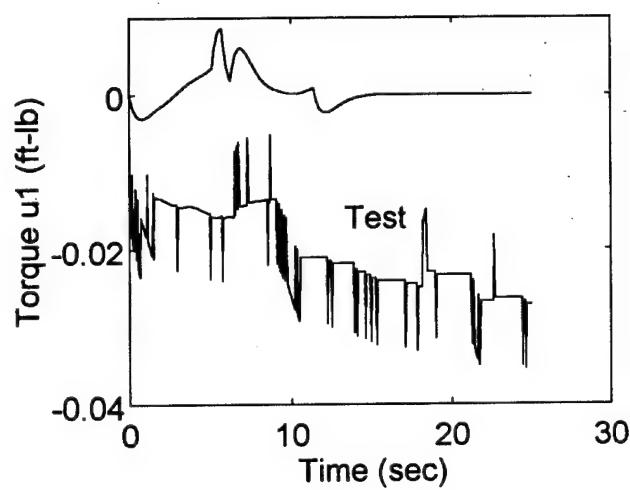
Fig. 11c
RESHAPE Maneuver:
25 deg Simulation and Test
du=0.08976 ft-lb
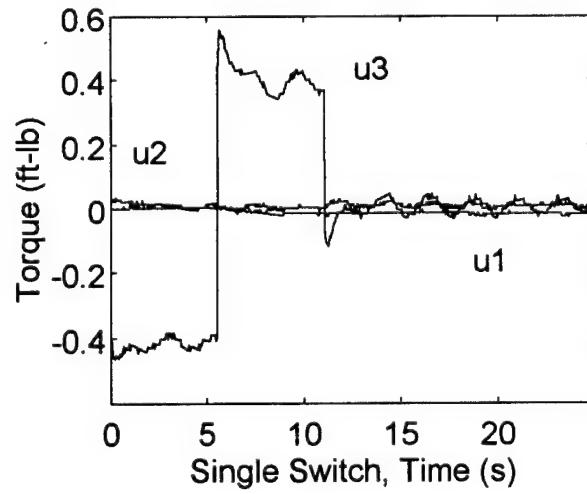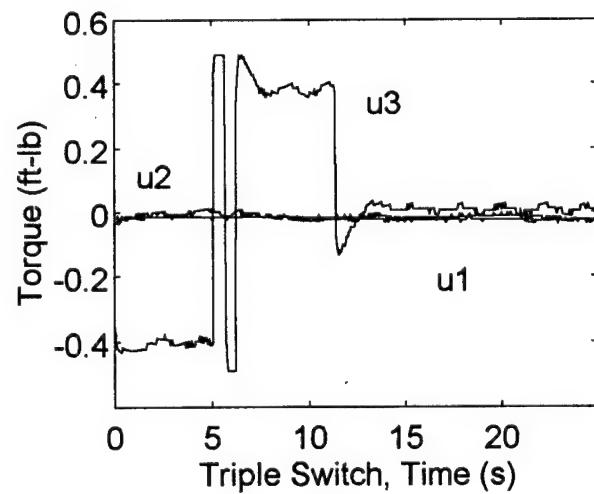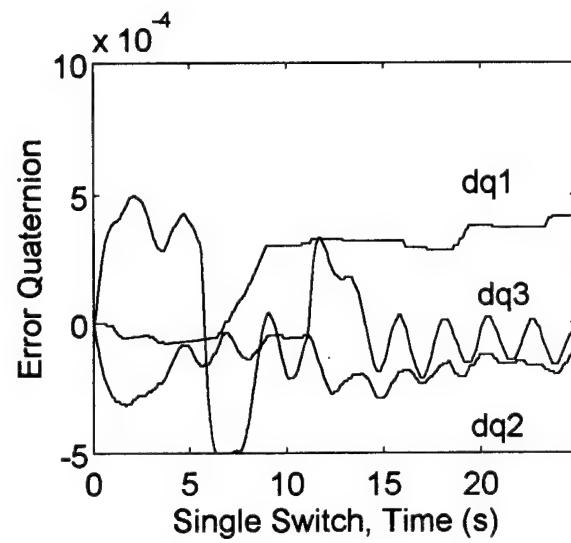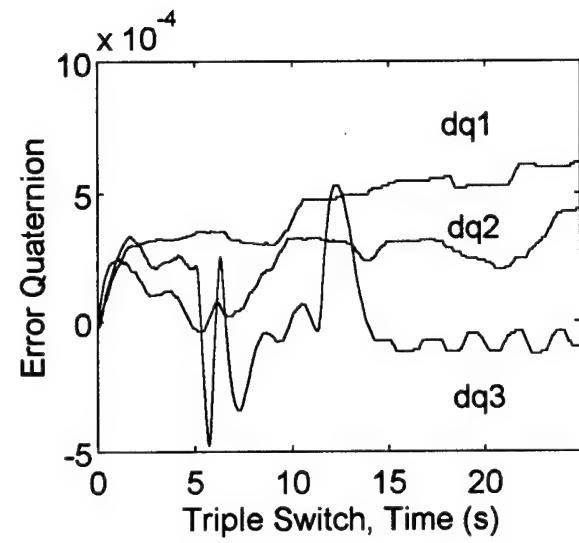
Fig. 12   RESHAPE Maneuver 25 deg Tests:
Single Switch Case: du3>0.08976 ft-lb;
Triple Switch Case: du3=0.08976 ft-lb;

3.33
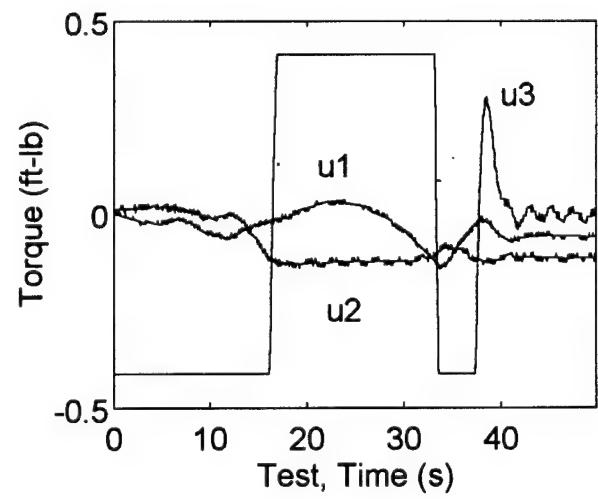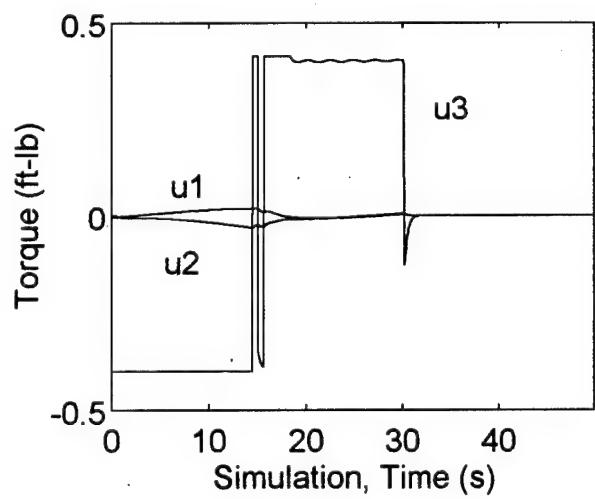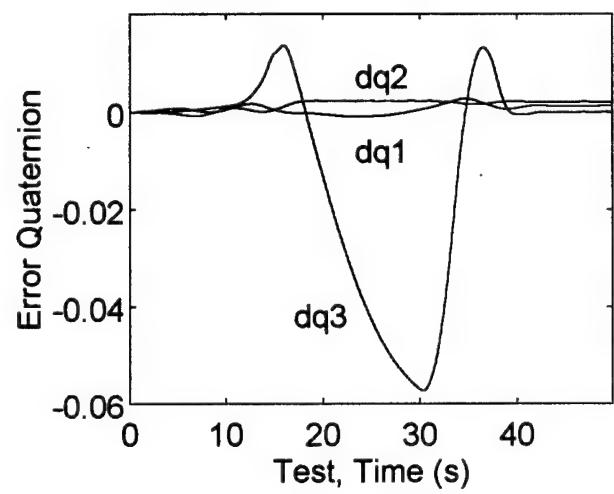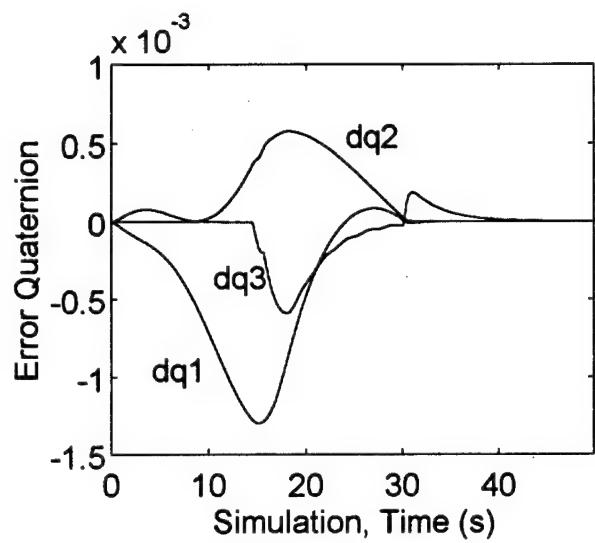
Fig. 13   RESHAPE Maneuver 180 deg Simulation and Test: du3=0.01056 ft-lb.

3.34
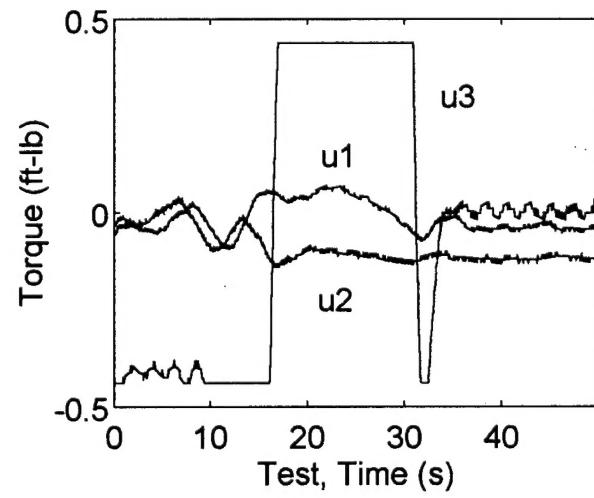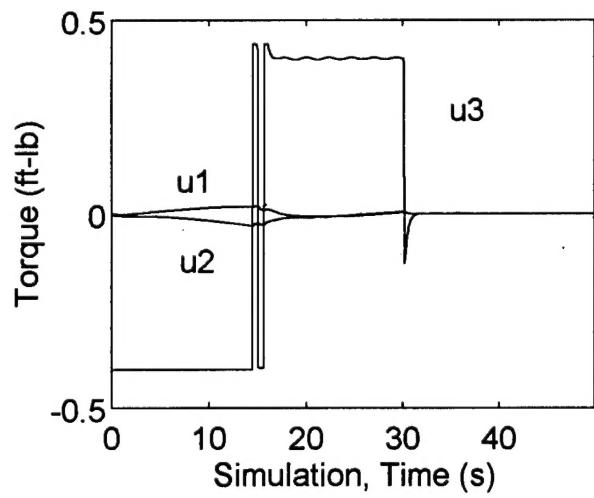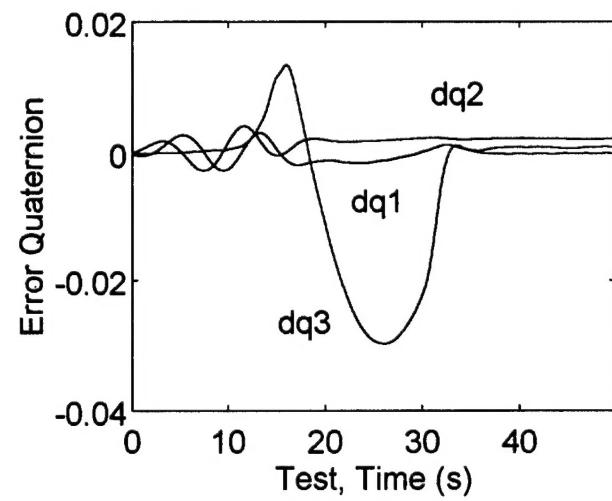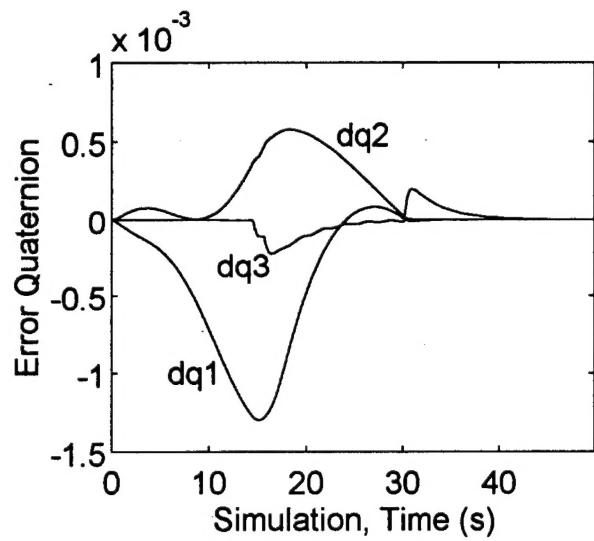
Fig. 14   RESHAPE Maneuver 180 deg Simulation and Test: du3=0.03696 ft-lb.
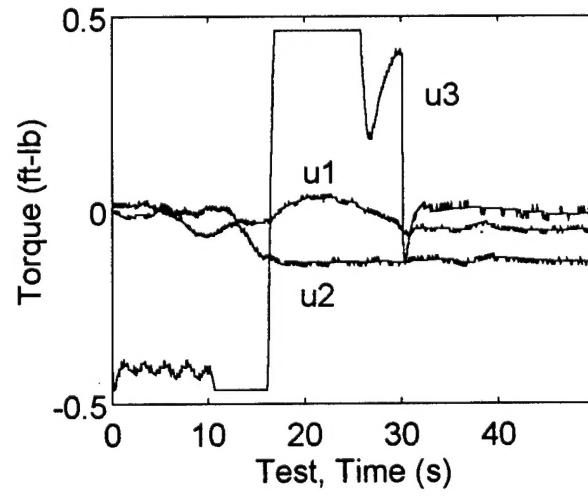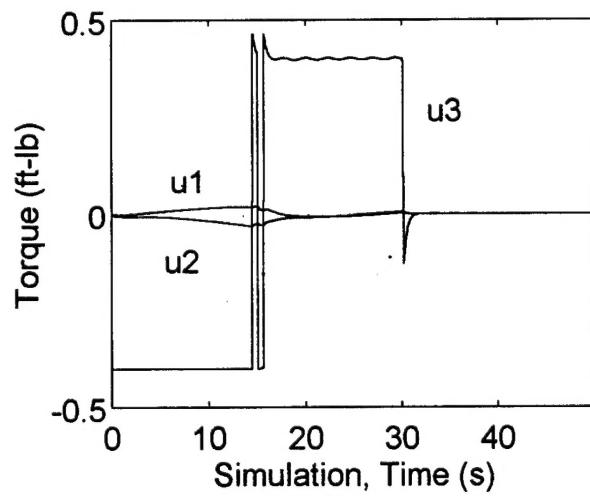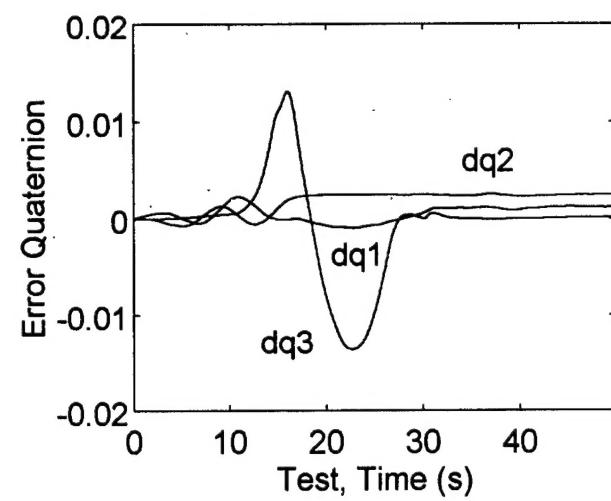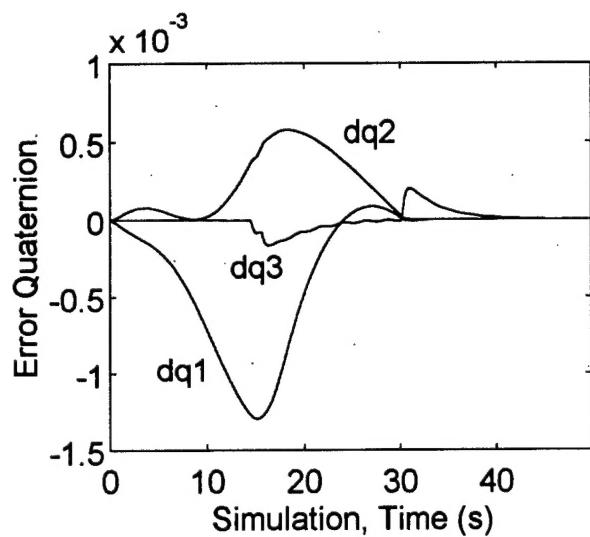
Fig. 15· RESHAPE Maneuver 180 deg Simulation and Test: du3=0.06336 ft-lb.

3.36

IV. CONCLUSIONS AND RECOMMENDATIONS

The effects of solar induced heating on a large, thin, shallow spherical shell in orbit are modelled mathematically. Such a structure would be representative of proposed orbiting antenna/reflector systems. For a 100 m. base radius shell made of polyamide a maximum thermal gradient of 3.6°C is predicted across the 1 cm shell thickness. As the system moves in its orbit the shell is alternately heated and cooled in a periodic manner due to the periodic change in the amount of solar radiation to which it is exposed. The shell is predicted to experience a maximum increase in its radius of curvature of 17m (nominal value, 5000 m) with smaller increases in its other dimensions. There is no corresponding significant increase in the solar radiation torque acting on the shell but there is a significant change in the shell's flexible vibrational frequencies. In fact for most of the first few modes the peak value of the frequency attained in the presence of solar-thermal effects is actually larger than the nominal frequency of the next highest mode. This means that when the mission requirements stipulate very accurate pointing and shape control that particular emphasis should be placed in the design of the controllers that limit the transverse vibrations.

Possible extensions to this work could consider the thermal shock problem encountered when the system transfers from the sunlit side of the orbit to the shadowed side and also the effect of local shadowing by different subsystem components on the rest of the system elements. Another extension to this work is to develop a model that could predict the solar-thermal effects on the tethered-shallow spherical shell-subsatellite system. This would represent an extension to the research reported in Chapter III of Volume I of this report, which emphasized the solar radiation effects on the tethered reflector sub-satellite system.

4.1

A practical bang-bang type and feedback control strategy for the minimum-time maneuver problem has been successfully applied for the first time to the Naval Research Laboratory's RESHAPE hardware test facility with a flexible pendulum-type appendage. The control strategy is based on the feed forward (open-loop solution) plus state-error feedback control. The open-loop solution is obtained by solving the related two-point boundary value problem using a shooting method. The success of this testing is shown by the excellent correlation between the numerical simulations and the experimental test results.

The technique developed here can be easily applied to other types of three-axis, nonlinear, and time-optimal maneuver experiements. It is suggested that this technique could be applied to more sophisticated hardware facilities such as the Phillips Laboratory's ASTREX faciility in the future. Unfortunately, during this AFOSR grant year it was not possible to schedule testing time with the original ASTREX facility at Edwards AFB although preliminary data was exchanged and numerical simulations were performed. Perhaps, with the relocation of the ASTREX faciility to Albuquerque, NM, another opportunity might be available. In addition to possible future testing with the ASTREX, three-axis slewing and vibration suppressionof the RESHAPE platform with other types of flexible appendages such as beams or antennas is recommended. Depending on the type of attachment of the appendages the effect of gravity may have to be compensated such as with the use of follower support cables and wires. Such devices would then have to be included in the RESHAPE system mathematical models, similar to the way that they are currently included in the ASTREX models.